Supporting Information Content

I. Mathematical Methods:

This section includes two modeling techniques: system identification (ID) models and physiological models. Figs. S1, S3 are schematics for the two techniques respectively; Fig. S2 shows HR response to both workload and ventilation; Fig. S4 shows results of the nonlinear optimal control for the static first principle model; and Fig. S5 shows HR response using the dynamic first principle model for the highest workload demand in Fig. 1.

II. Simulation Results for all Experimental Subjects:

Figs.S6-S20 show simulation results of applying the two techniques to the five subjects' data.

III. Nonlinear Dynamic Models from System ID:

A global nonlinear model is fit to explain the overall response of HR to a broad range of power generation. Fig. S21 shows the simulation result.

IV. Cross Validation:

Figs.S22-S23 and Table S1 show cross validation results for linear system identification; Fig. S24 shows cross validation results for the physiological modeling; Figs. S25-S26 shows cross validation results for the nonlinear system identification.

V. Tables S2-S4:

Tables S2-S4 provide the necessary parameter values in the simulation.

VI. System Identification Techniques:

A pure technical introduction on system identification is provided.

Supporting Information

I. Mathematical Methods

1. System Identification Model

System identification begins with measurements of the behavior (output) of the system when external influences are imposed (i.e. inputs to the system), and then determines a mathematical model for this interaction without going into the details of what is actually happening inside the system. Though there exist many sophisticated numerical methods to identify a linear time invariant (LTI) dynamic system in order to fit observed input-output data, in general, it is difficult to mathematically characterize a complicated dynamic system, e.g. nonlinear system or a high order system. To minimize the complexity of the requisite model and numerical methods, this paper mainly uses low order LTI models in observable canonical form [33]. However, the entire physiological body system is a complex and not necessarily linear system. Therefore we carefully designed the experiments to ensure that the LTI model can provide a good approximate to the true system for each experiment.

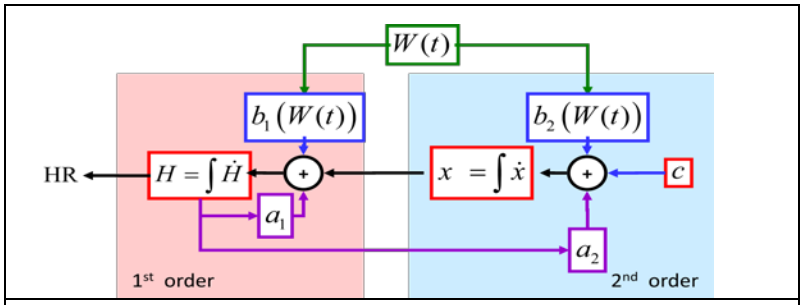

Figure S1: System Identification schematic

As an example, a 2nd order linear model in observable canonical form is shown as follow:

$$\begin{aligned} \Delta H(t) &= a_1 H(t) + b_1 W(t) + x(t) \\ \Delta x(t) &= a_2 x(t) + b_2 W(t) + c \end{aligned} \quad \text{(SI-1)}$$

where a_1, a_2, b_1, b_2, c are constants, W (workload power or ventilation) is the input signal, H (HR) is the output signal, and x is an internal state. In **Fig. 7**, we apply simple nonlinear models to fit the data for anaerobic exercise by using workload power as input. The nonlinear models have the same structure as (SI-1) except that $b_i \cdot W(t)$ is changed to be a piecewise linear function $b_i(W(t))$ in the form of (A schematic is shown in Fig. S1.):

$$b_i(W(t)) = \begin{cases} b_{i,1} \cdot W(t) & \text{if } W(t) \le 220 \text{ watts} \\ b_{i,2} \cdot W(t) & \text{else} \end{cases}$$

Given a certain order of this structure, we use nonlinear programming techniques [33] to search for parameter values that minimize the mean squared error between measured HR and simulated HR (H). We then iterate to find an order that gives a reasonable tradeoff between model complexity (order) and simulation error. Using observable canonical form reduces the search dimension of the nonlinear program without loss of generality. For readers unfamiliar with these methods, we provide a more technical introduction on system identification in SOM-Section VIII: *System Identification Techniques.*

We also use both workload W and ventilation V data as inputs to fit HR data during the easy workout in **Fig. 1**. Fig. S2 shows the output H (in black) of a simple 2-state, 7-parameter linear model with both W and V as inputs

$$\begin{aligned} \Delta H(t) &= a_1 H(t) + b_1 V(t) + d_1 W(t) + x(t) \\ \Delta x(t) &= a_2 x(t) + b_2 V(t) + d_2 W(t) + c \end{aligned}$$

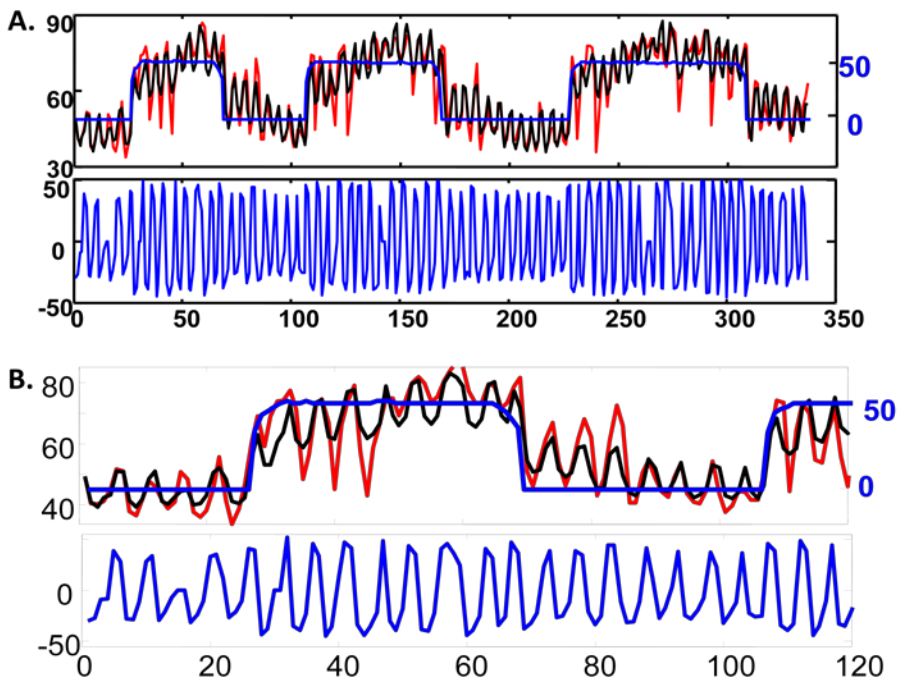

Figure S2: **HR response to both workload and ventilation: (A)** HR (red) and dynamic fit (black) to inputs of workload (blue in the top figure) and natural ventilation (blue in the lower figure); **(B)** is a zoomed in version of (A).

2. First Principle Model

In this section, we will focus on establishing the 1st principle model in Equation (2-4) and explain how we carried out the static and dynamic analysis (**Figs. 3-4**) using this physiological model.

The block diagram of the basic circulatory system is shown in Fig. S3 [32]. The basic task of the cardiovascular system is to satisfy metabolic requirement for O_2, glucose, and other nutrients while simultaneously removing CO_2 and the other end products of metabolism. To fulfill these tasks, the heart pumps blood through the pulmonary circuit and the systemic circuit. The heart consists of four chambers of two types: atria and ventricles. For simplicity, we will refer to the right atrium and right ventricle as the right heart, and the left atrium and left ventricle as the left heart. The left heart receives blood from the lungs which is rich in O_2, and pumps it into the systemic arteries distributing O_2 and metabolic substrates to end-organs. Metabolic end products are removed as O_2-depleted blood leaves the systemic peripheral tissues, enters the central venous compartment and returns to the right heart. The right heart pumps blood into the

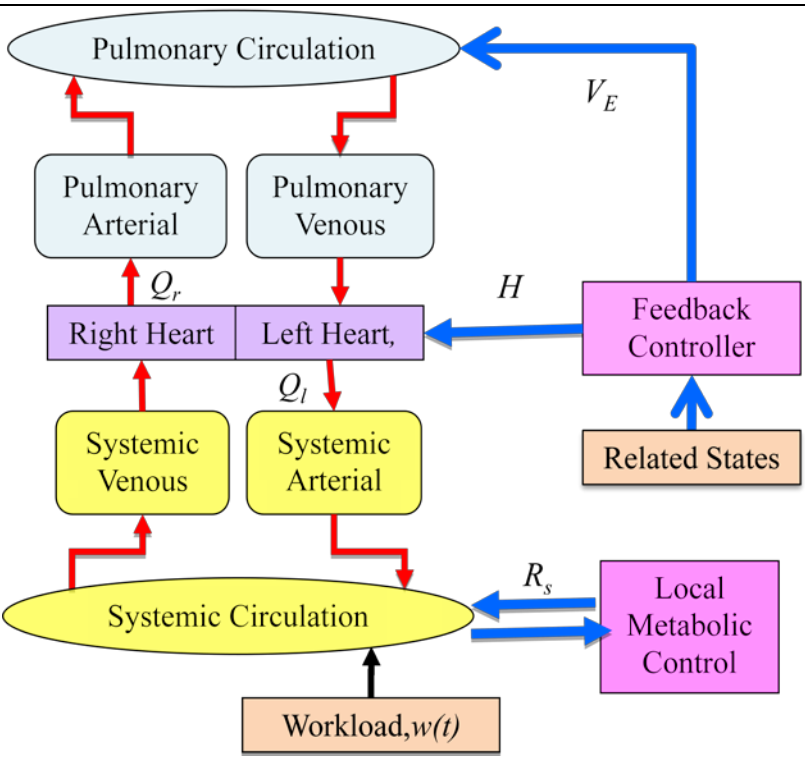

Figure S3: Block diagram of the basic cardiovascular model [32].

pulmonary arterial circulation, where O_2 is taken up from alveoli and CO_2 is transferred to alveoli and exhaled. Blood returns to the left heart via the pulmonary veins. The variables in the figure are explained in the following sections.

Our model is based on the circulatory circuit diagram, using standard mathematical descriptions of circulation, with a focus on modeling purely aerobic exercise. We only model blood flow and O_2 and we do not model CO_2, pH, glucose and other variables. CO_2 and pH are important signals, but during aerobic exercise in young, fit adults, changes in CO_2 correlate with changes in O_2 such that any signal that depends on CO_2 is approximately a function of O_2. Moreover, during short aerobic exercise, pH is almost constant. By modeling blood flow and O_2, the model captures the overall physiologic response during low level exercise in young, fit adults.

2.1 Basic Model

2.1.1 Blood Circulation Model

The circulation of blood is described by well-established models [27-32]. Here we build a simple model based on the models developed in Peskin *et al.* [31] and Batzel *et al.* [32] to explain cardiovascular control systems.

We distinguish four compartments of the circulatory system, i.e., the arterial and venous compartments of the systemic and pulmonary circuits, treating each compartment as a compliant vessel with no resistance to blood flow. That is, we assume that blood volume in the compartment is determined by pressure in the compartment. A simple linear relationship between pressure and volume in such a compartment is assumed:

$$\begin{aligned} V_{as} &= c_{as} P_{as} \\ V_{vs} &= c_{vs} P_{vs} \\ V_{ap} &= c_{ap} P_{ap} \\ V_{vp} &= c_{vp} P_{vp} \end{aligned}$$

V variables are volumes, P variables are pressures, and c is the compliance for a=arterial, v=venous, s=systemic, and p=pulmonary compartments.

The rate of change for the volume V in a compartment is the difference between the flow into and flow out of the compartment, described by the following equations:

$$\begin{aligned} c_{as}\dot{P}_{as} &= \dot{V}_{as} = Q_l - F_s \\ c_{vs}\dot{P}_{vs} &= \dot{V}_{vs} = F_s - Q_r \\ c_{ap}\dot{P}_{ap} &= \dot{V}_{ap} = Q_r - F_p \\ c_{vp}\dot{P}_{vp} &= \dot{V}_{vp} = F_p - Q_l \end{aligned} \qquad \text{(SI-2)}$$

Q variables are the cardiac outputs for l=left heart and r=right heart; F variables are the blood flow for s= systemic and p= pulmonary circulation. We will establish models for cardiovascular output Q and blood flow F in the following parts.

Cardiovascular output

Cardiac output is a function of heart rate (H) and stroke volume (V_{str}), the amount of blood pumped with each cardiac contraction:

$$Q_{co} = HV_{str} \qquad \text{(SI-3)}$$

and $V_{str} = V_{diast} - V_{syst} = c_{diast}P_v - c_{syst}P_a$.

Here we regard the ventricle as a compliance vessel in which compliance changes over time. V_{diast} is end-diastolic blood volume of the relaxed ventricle and V_{syst} is the end-systolic blood volume of the maximally contracted ventricle. P_a is the pressure in the arteries supplied by the ventricle and P_v is the pressure in the veins that fill it. Usually c_{syst} is very small and c_{diast} is much larger. A simple special case when $c_{syst} = 0$ yields a description of stroke volume:

$$V_{str} = c_{diast}P_v \qquad \text{(SI-4)}$$

Combining equations (SI-3) and (SI-4) describes cardiac output for the left and right heart respectively:

$$\begin{aligned} Q_r &= c_r \cdot H \cdot P_{vs} \\ Q_l &= c_l \cdot H \cdot P_{vp} \end{aligned} \qquad \text{(SI-5)}$$

c_r and c_l are c_{diast} for the right and left heart respectively.

Blood Flow in the Circulation

We assume that the systemic and pulmonary circulation acts like a pure resistance vessel to blood flow. By Ohm's law,

$$\begin{aligned} F_s &= (P_{as} - P_{vs}) / R_s \\ F_p &= (P_{ap} - P_{vp}) / R_p \end{aligned} \quad \text{(SI-6)}$$

where *R* variables represent resistance to blood flow.

In our model, we assume that the pulmonary resistance R_p is a constant parameter, while the peripheral resistance R_s is decreased during exercise and the decrease is determined by local metabolic control. The purpose of decreasing peripheral resistance in the arterioles is to increase blood flow and regional delivery of O_2, glucose, and other substrates as needed. With exercise, local dilation of the arterioles is triggered by local release of vasodilating factors. We assume that peripheral resistance R_s is determined as [31]:

$$R_s = A \cdot [O_2]_v + R_{s0} \quad \text{(SI-7)}$$

A and R_{s0} are two constants; and $[O_2]_v$ is the tissue oxygen content which will be introduced later.

Blood Pressure Model

Assuming a constant total blood volume V_{tot}:

$$V_{as} + V_{vs} + V_{ap} + V_{vp} = V_{tot} \quad \text{(SI-8)}$$

Combining equations (SI-2), (SI-5), (SI-6), (SI-8) yields the following dynamic blood circulation model:

$$\begin{aligned} c_{as}\dot{P}_{as} &= c_l \cdot H \cdot P_{vp} - \left(P_{as} - P_{vs}\right) / R_s \\ c_{vs}\dot{P}_{vs} &= \left(P_{as} - P_{vs}\right) / R_s - c_r \cdot H \cdot P_{vs} \\ c_{ap}\dot{P}_{ap} &= c_r \cdot H \cdot P_{vs} - \left(P_{ap} - P_{vp}\right) / R_p \\ c_{vp}P_{vp} &= V_{total} - \left(c_{as}P_{as} + c_{vs}P_{vs} + c_{ap}P_{ap}\right) \end{aligned} \quad \text{(SI-9)}$$

Note that the equation for P_{vp} is not a dynamic equation.

2.1.2 Tissue Oxygen Transport Model

The equation describing oxygen exchange in the tissue compartment is [29-32]:

$$v_{T,O_2}[\dot{O}_2]_T = -M + F_s([O_2]_a - [O_2]_v) \quad \text{(SI-10)}$$

The left hand side of the equation represents the change in O_2 content across the tissue compartment, which is calculated by multiplying the fixed effective O_2 volume v_{T,O_2} with the

change in O_2 content $[O_2]_T$. The right hand side of the equation describes the net volume changes in terms of the metabolic consumption of O_2 denoted by *M* and its supply described by the net change in the arterial and venous blood O_2 contents denoted, respectively, by $[O_2]_a$ and $[O_2]_v$.

We use the following empirical formula for the resulting metabolic rate *M*:

$$M = \rho \cdot W + M_0$$

where W is the ergometric workload imposed on the subject during exercise, M_0 is the metabolic rate in systemic tissue corresponding to zero workload and ρ is a positive constant parameter. Moreover, we assume that tissues and venous blood gases are in equilibrium; tissue oxygenation $[O_2]_T$ is the same as venous oxygenation $[O_2]_v$, i.e.

$$[O_2]_T = [O_2]_v$$

2.1.3 The Basic Model

Equations (SI-9), (SI-10) are combined to be the first principle model with 4 states and 1 unknown controllers:

$$\begin{aligned}
c_{as}\dot{P}_{as} &= c_l \cdot H \cdot P_{vp} - (P_{as} - P_{vs}) / R_s \\
c_{vs}\dot{P}_{vs} &= \left(P_{as} - P_{vs}\right) / R_s - c_r \cdot H \cdot P_{vs} \\
c_{ap}\dot{P}_{ap} &= c_r \cdot H \cdot P_{vs} - (P_{ap} - P_{vp}) / R_p \\
v_{T,O_2}[\dot{O}_2]_v &= -(\rho \cdot W + M_0) + F_s \cdot \left(\left[O_2\right]_a - \left[O_2\right]_v\right) \qquad \text{(SI-11)} \\
c_{vp}P_{vp} &= V_{total} - \left(c_{as}P_{as} + c_{vs}P_{vs} + c_{ap}P_{ap}\right) \\
R_s &= A \cdot [O_2]_T + R_{s0} \\
H &= u(\cdot)
\end{aligned}$$

where $u(\bullet)$ is the control function of heart rate *H*. The model describes a 4-state nonlinear dynamic system (again, note that the equations for P_{vp} and R_s are not dynamic equations.). We will describe how to determine the control function below.

2.2 Control Mechanisms

The cardiovascular control system is complex and has been studied intensively [27, 28, 32], but unresolved questions and controversies about HR control and HRV persist. Homeostasis is manifested in healthy physiological states, meaning that steady state behavior is maintained despite varying inputs to the system [4, 5, 27, 28, 32]. The physiologic response to perturbations

(such as exercise in our study) reveals the dynamic behavior of the control systems that maintain homeostasis.

Exercise is an important physiologic perturbation. The control objective of normal physiology is to produce sufficient energy for muscle activity, while maintaining critical biologic parameters within an acceptable range. Ventilation, vascular resistance, and blood flow are the primary factors that govern operation of the cardiopulmonary system, maintaining a tradeoff between energy production requirements and physiological equilibrium. In order to deliver sufficient O_2 during exercise, ventilation increases, cardiac output rises and skeletal muscle arterioles dilate. The magnitude of these responses is bounded in order to remain acceptable close to equilibrium. The degree to which they are bounded highlights how the cardiopulmonary system manages this tradeoff. Critical physiologic variables must be controlled so that actual structural damage is prevented [27, 28, 32]. The arterial partial pressure of oxygen, P_{a,O_2}, is the key regulated variable with a set-point of ~100 mm Hg. As a result of this tight control on P_{a,O_2}, the hemoglobin in systemic arterial blood is kept saturated with oxygen yielding (in the absence of anemia) a systemic arterial oxygen content $[O_2]_a$ of around 20 ml O_2/100 ml blood. This is demonstrated by the nearly constant SpO_2 value which is maintained during exercise, an observation supported both by the literature and our experimental data. In addition, the arterial partial pressure P_{as} is controlled by the baroreceptor loop, a short-term feedback control mechanism.

The intent here is not to model the entire circulatory control system in detail. Instead, we focus on nervous system control over heart rate *H* to guarantee "sufficient oxygen" and maintain P_{as} at a certain level. Rather than model the control system in detail, we construct a feedback controller which regulates heart rate based on several important system state variables, e.g. blood pressure, oxygen saturation, energy reserve. Here, we assume that the objective of the cardiovascular control system is to stabilize/balance those important variables around their (pre-)defined/safe values as well as to minimize the work done by the heart. Thus the loop can be considered as a stabilizing and optimizing feedback. We will carry out steady state analysis first and then explain the dynamical cases.

Before carrying out the analysis, we simplify notations by defining the state vector:

$$s = (P_{as}, P_{vs}, P_{ap}, [O_2]_v)^T \in R^4$$

and the parameter vector,

$$p = (c_{as}, c_{vs}, c_{ap}, c_{vp}, c_l, c_r, V_{tot}, R_p, R_{s0}, [O_2]_a, A, \rho, M_0, V_{T,O_2})^T \in R^{14} \quad \text{(SI-12)}$$

Then the model (4-state nonlinear system) can be defined as:

$$\dot{s} = F(s(t), p, W, H)$$

In the following analysis, we shall not fit the parameter vector *p* in (SI-12), but instead, we take physiologic nominal values from the literature for all parameters *p,* which is shown in Table 2-3. For all experimental subjects, we use the same parameter values for *p* except for the two parameters of cardiac output, c_l and c_r . For these, we use larger values for the larger subjects. The parameters that we fit will be introduced later.

Static Analysis

To obtain a steady state model for the cardiovascular system, we set the right side of equation (11) to be 0, and solve for mean systemic arterial blood pressure and oxygen saturation as a function of heart rate and workload, (P_{as}, ΔO_2)=*f*(*H*,*W*), where P_{as} is the mean systemic arterial blood pressure and ΔO_2 is $[O_2]_a - [O_2]_T$:

$$\begin{aligned} P_{as} &= \frac{(V_{tot} + c_{as} \cdot M_{O_2} \cdot A) \cdot (1 + c_r \cdot A \cdot [O_2]_a \cdot H + c_r \cdot R_s \cdot H)}{c_r \cdot B + (c_{as} \cdot A \cdot [O_2]_a + c_{as} \cdot R_{s0} + c_{ap} \cdot R_p) \cdot c_r \cdot H} - A \cdot M_{O_2} \\ \Delta O_2 &= \frac{M}{V_{tot} + c_{as} \cdot M_{O_2} \cdot A} \cdot \left(c_{as} \cdot A \cdot [O_2]_a + c_{as} \cdot R_{s0} + c_{ap} \cdot R_p + B / H \right) \end{aligned} \quad \text{(SI-13)}$$

where $B = \frac{c_{as}}{c_r} + \frac{c_{vs}}{c_r} + \frac{c_{ap}}{c_l} + \frac{c_{vp}}{c_l}$. Using the two equations, we get the mesh plot in Fig 3.

As discussed above, we model the regulation on *H* as optimal feedback control to minimize the deviation of the important physiologic variables from normal resting values. Mathematically, the optimal *H* is solved by minimizing the following objective function:

$$\min \; q_P \left(P_{as} - P_{as}^* \right)^2 + q_{o_2} \left(\Delta O_2 - \Delta O_2^* \right)^2 + q_H \left(H - H^* \right)^2 \quad \text{(SI-14)}$$

Here q_P, q_{o_2}, q_H are weighting factors and $P_{as}^*, \Delta O_2^*, H^*$ are steady values for $P_{as}, \Delta O_2, H$ at the referenced workload level W^*.

To solve the optimization problem, we linearize the two equations in (SI-13) for P_{as}, ΔO_2 around the referenced point ($P_{as}^*, \Delta O_2^*, H^*, W^*$) and get the following two linear expressions for P_{as}, ΔO_2:

$$P_{as} - P_{as}^* = a_1 \cdot (H - H^*) + b_1 \cdot (W - W^*)$$
$$\Delta O_2 - \Delta O_2^* = a_2 \cdot (H - H^*) + b_2 \cdot (W - W^*)$$

Then given a tradeoff weighting vector $\left(q_P, q_{O_2}, q_H\right)$, we can solve the optimization problem (SI-14) and the result is in the form of $H - H^* = b_3 \cdot (W - W^*)$. By tuning the tradeoff weighting vector $\left(q_P, q_{O_2}, q_H\right)$, we are able to get a physiologically plausible solution which is shown as the solid line in **Fig. 3**. The tradeoff weighting vector $\left(q_P, q_{O_2}, q_H\right)$ is set as follows:

- W=0~110watts: q_P =3, q_{O_2} =10^7, q_H =3;
- W=110~250watts: q_P =6, q_{O_2} =10^7, q_H =6;

The different q values reflect different tradeoffs between P_{as}, O_2, and HR as workload increases.

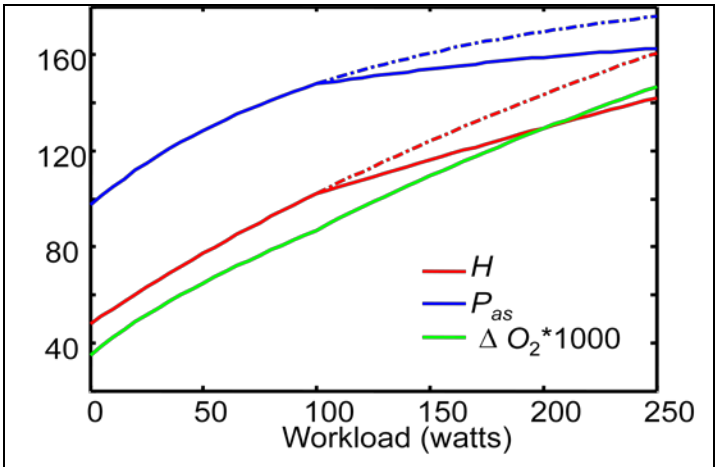

Figure S4: Nonlinear optimal control for static 1st principle model (HR: red; P_{as}: blue; ΔO_2 : green). Solid lines are the solutions by changing trade-off weight vectors between 0~110 watts and 110~250 watts. Dashed lines are the hypothetical solutions by using the same trade-off weight vectors for 110~250 watts as 0~110 watts.

We can also solve the optimization problem in (SI-14) without doing any linearization. Substituting (P_{as}, ΔO_2)=$f(H,W)$ in (SI-13) into the objection function in (SI-14), the optimization problem (SI-14) becomes a non-constrained optimization problem with the objective function in terms of H and W. Given the trade-off weighting vectors $\left(q_P, q_{O_2}, q_H\right)$, we can solve the optimization problem and find the optimal controller for H in terms of $h(W)$

which is a nonlinear function. By tuning the tradeoff weighting vector $\left(q_P, q_{O_2}, q_H\right)$, we are able to get a physiologically plausible solution which is shown in Fig. S4. The tradeoff weighting vector $\left(q_P, q_{O_2}, q_H\right)$ is set as follows:

- W=0~110watts: q_P =2, q_{O_2} =10^7, q_H =1.5;
- W=110~250watts: q_P =4, q_{O_2} =10^7, q_H =4;

Notice that we do not fit parameter vector p in (SI-12), but instead we just tune the tradeoff weighting vector. This means the model is over-determined and we require few parameters to fit the data, consistent with our findings based on system identification techniques. Fitting the tradeoff weighting vector in cost function ensures appropriate input-output behavior and has a physiologically plausible interpretation since it can determine how much each individual physiological term influences the cardiovascular control system.

Dynamic Analysis

Next, we determine the controller *u(.)* in the dynamic model (SI-11). Here, we assume that the objective of the cardiovascular control system is to quickly and sufficiently stabilize important physiologic variables to (pre-)defined/safe levels. Mathematically this can be obtained by minimizing the following cost function:

$$J(u(\cdot)) = \int_0^\infty \left(q_P^2 \left(P_{as}(t) - P_{as}^* \right)^2 + q_{O_2}^2 \left(\Delta O_2 - \Delta O_2^* \right)^2 + q_H^2 \left(H - H^* \right)^2 \right) dt \quad \text{(SI-15)}$$

Here q_P, q_{o_2}, q_H are weighting factors and $P_{as}^*, \Delta O_2^*, H^*$ are steady values for $P_{as}, \Delta O_2, H$ at the referenced workload level W^*.

In each interval exercise experiment shown in Fig. 4, there are two exercise levels. For each interval test, there is a steady state value s^* corresponding to the lower level workload. We introduce the transformation $\xi(t)=s(t)-s^*$ and linearize the model (SI-11) around $\xi = 0$:

$$\dot{\xi}(t) = A\xi(t) + B(H(t) - H^*), \qquad t \geq 0$$
$$\xi(0) = s(0) - s^*,$$

where

$$A = \left.\frac{\partial F(s, p, W, H)}{\partial s}\right|_{s=s^*, W=W^*, H=H^*}$$

$$B = \left.\frac{\partial F(s, p, W, H)}{\partial H}\right|_{s=s^*, W=W^*, H=H^*}$$

H^* and W^* are corresponding heart rate and workload for the lower exercise level in each interval exercise test, which is 0 watts and 100 watts in our case.

Defining $C = (q_P, 0, 0, q_{O_2})$, the cost function (SI-15) takes on the form:

$$J(u(\cdot)) = \int_0^\infty \left(C\xi(t)\right)^2 + \left(q_H \hat{u}(t)\right)^2 dt$$

where $\hat{u}(t) = H(t) - H^*$. From control theory [34], the solution of this linear-quadratic regulator problem is given by a linear feedback law (*32*):

$$\hat{u}(t) = -K\xi(t),$$

where K is given by:

$$K = q_H^{-1} B^T P$$

and P is found by solving the continuous time algebraic Ricaati equation

$$A^T P + PA - PBq_H^{-1} B^T P + C^T C = 0$$

Therefore we obtain the controller on heart rate H in the following form:

$$H(t) = u(t) = \hat{u}(t) + H^l = -K\xi(t) + H^l.$$

As we do in static analysis, we fit the weighting vector q_P, q_{o_2}, q_H instead of fitting the parameter vector p to get the simulation results shown in Fig. 4. For different interval exercises, we have different q values. Those q values for different interval exercises reflect different tradeoffs between P_{as}, O_2, H, as their means increase. For each subject, those q values are shown in Table 4 and the corresponding simulation results are shown in SOM-Section II: *Simulation Results for all Experimental Subjects*.

However, if we apply this 1st principle aerobic model for the highest interval test in **Fig. 1**, the best simulation results we can obtain by tuning the weighting vector q is shown in Fig. S5, from which we can see that our aerobic model fails to capture most HR dynamics for anaerobic exercise.

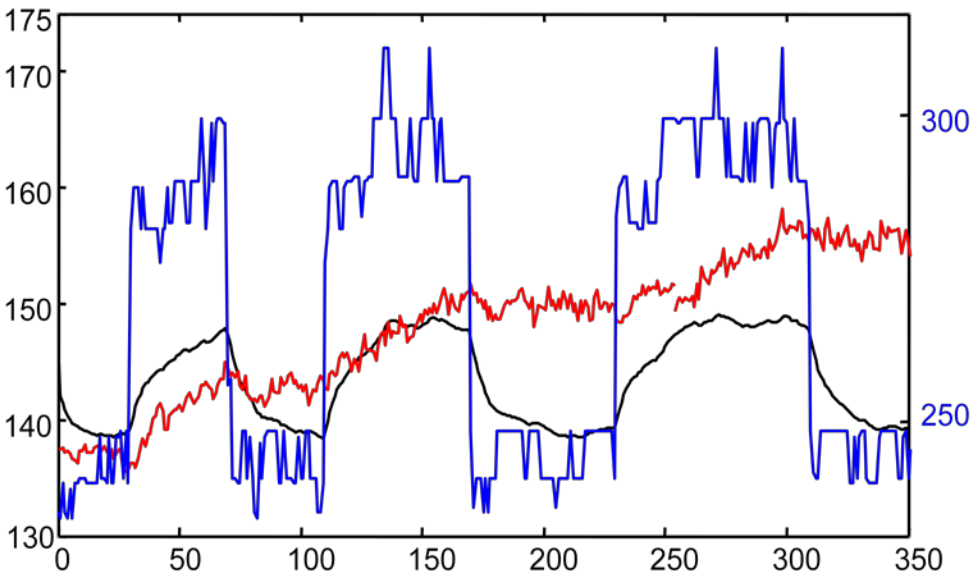

Figure S5: **HR response using 1st principle model for the highest workload (blue) demand in Fig. 1**. A physiological model with optimal controller is simulated with workload as input (blue) and HR (black) as output, and compared with collected HR data (red).

II. Simulation Results for all Experimental Subjects

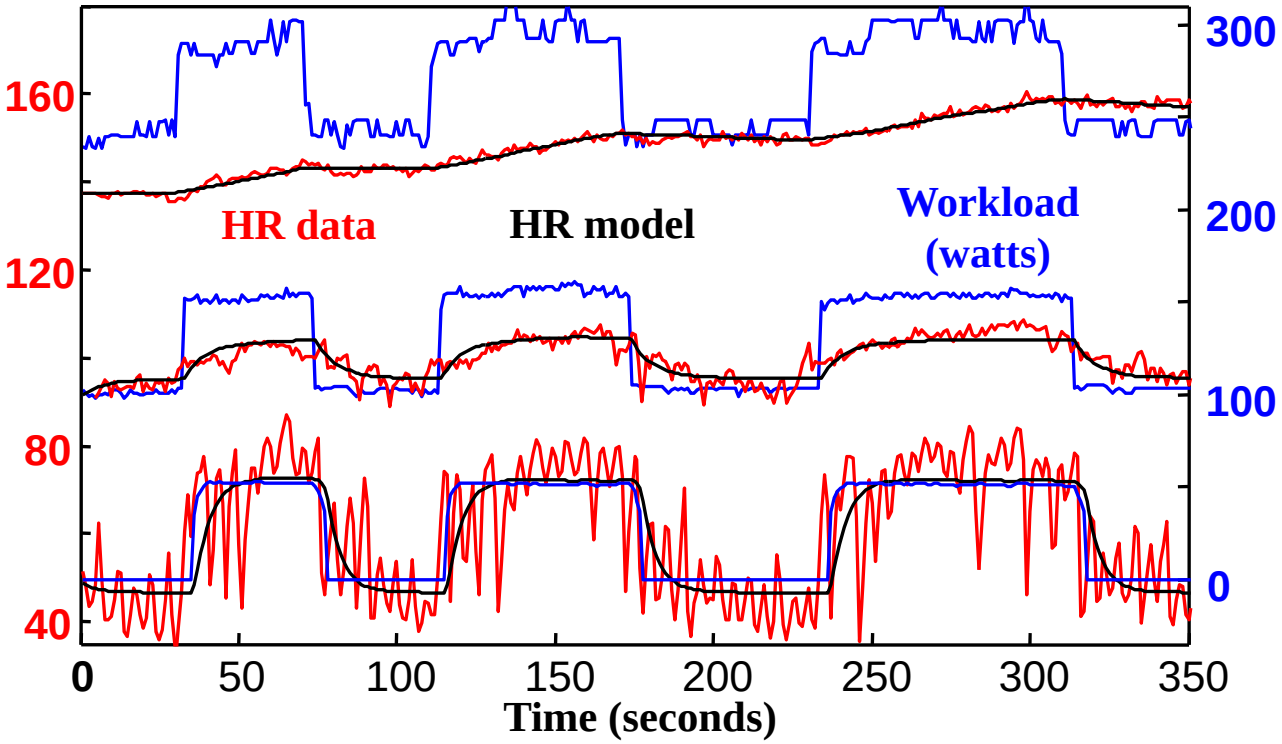

Figure S6: Subject #1 performed three separate experiments of less than 6 minutes each on a cycle ergometer. HR (left axis, red) is plotted for three different workload demands (right axis, blue). The workload profiles are similar but shifted square waves of 0-50 watts (lower), 100-150 watts (middle), and 250-300 watts (upper). A one state linear dynamic ("black box") model with 3 parameters (different for each case) was fit using workload input and HR output. The optimal parameter values (a, b, c)≈ (-0.22, 0.11, 10.2) at 0 watts differ greatly from those at 100 watts (-0.06, 0.012, 4.6) and at 250 watts (-0.003, 0.003, -0.27). Simulations of these 3 different models with the 3 corresponding workload inputs are in black. Breathing was spontaneous (not controlled), and SpO_2 was essentially constant throughout.

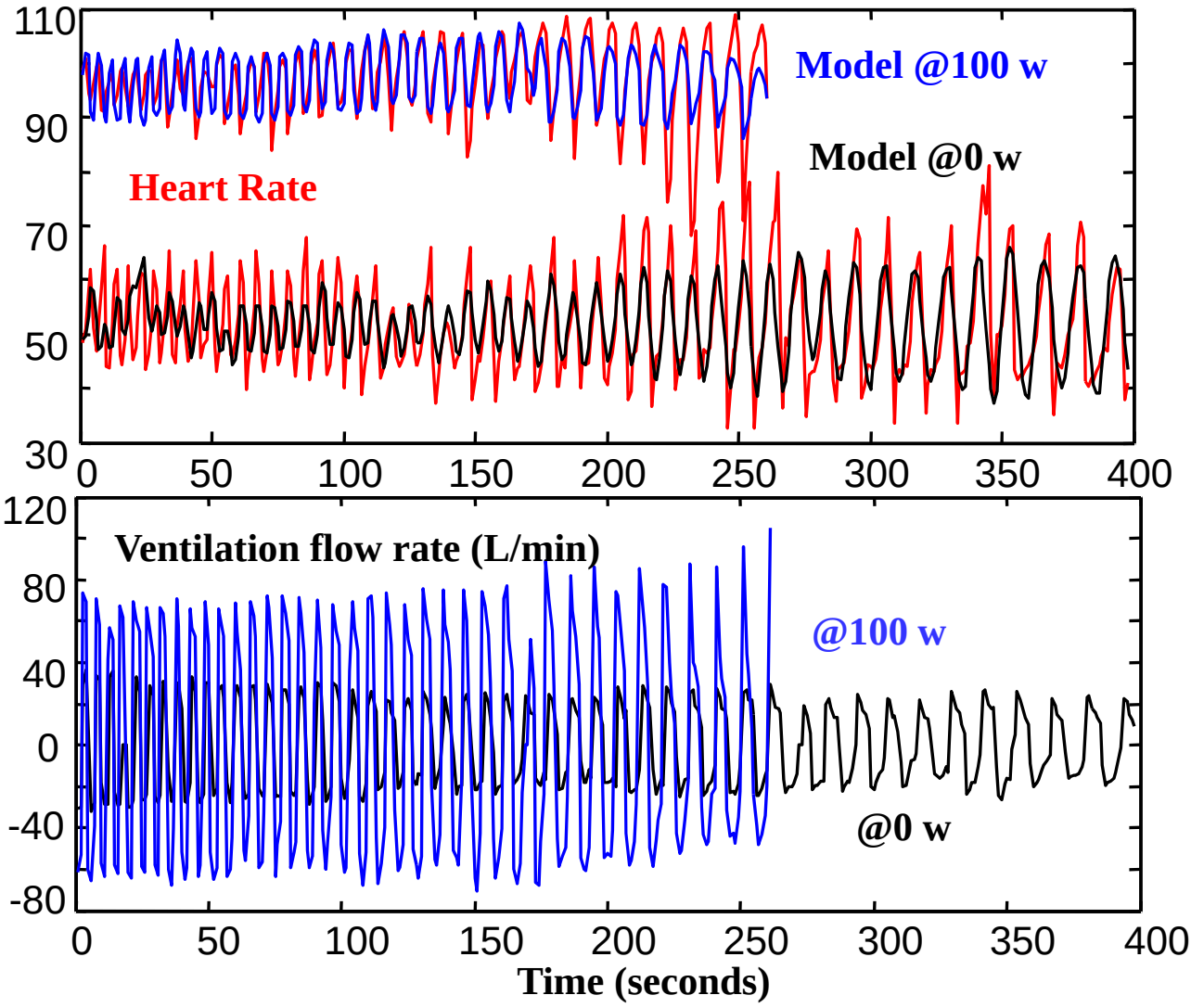

Figure S7: Subject #1's data: two experiments with input of controlled frequency sweeps in ventilation flow rate (lower plot) with fixed background workload demand of 0 watts (black) or 100 watts (blue). Subject #1 controlled breathing to follow a preprogrammed frequency sweep that spanned the natural breath frequencies at these workload levels. The ventilation data are raw speed of inhalation and exhalation at the mouthpiece. For each data set, a second order linear model was fit with airflow rate input (lower plot) and HR output (upper, data in red). Simulations of HR are in upper plot for 0 watts (black) and 100 watts (blue).

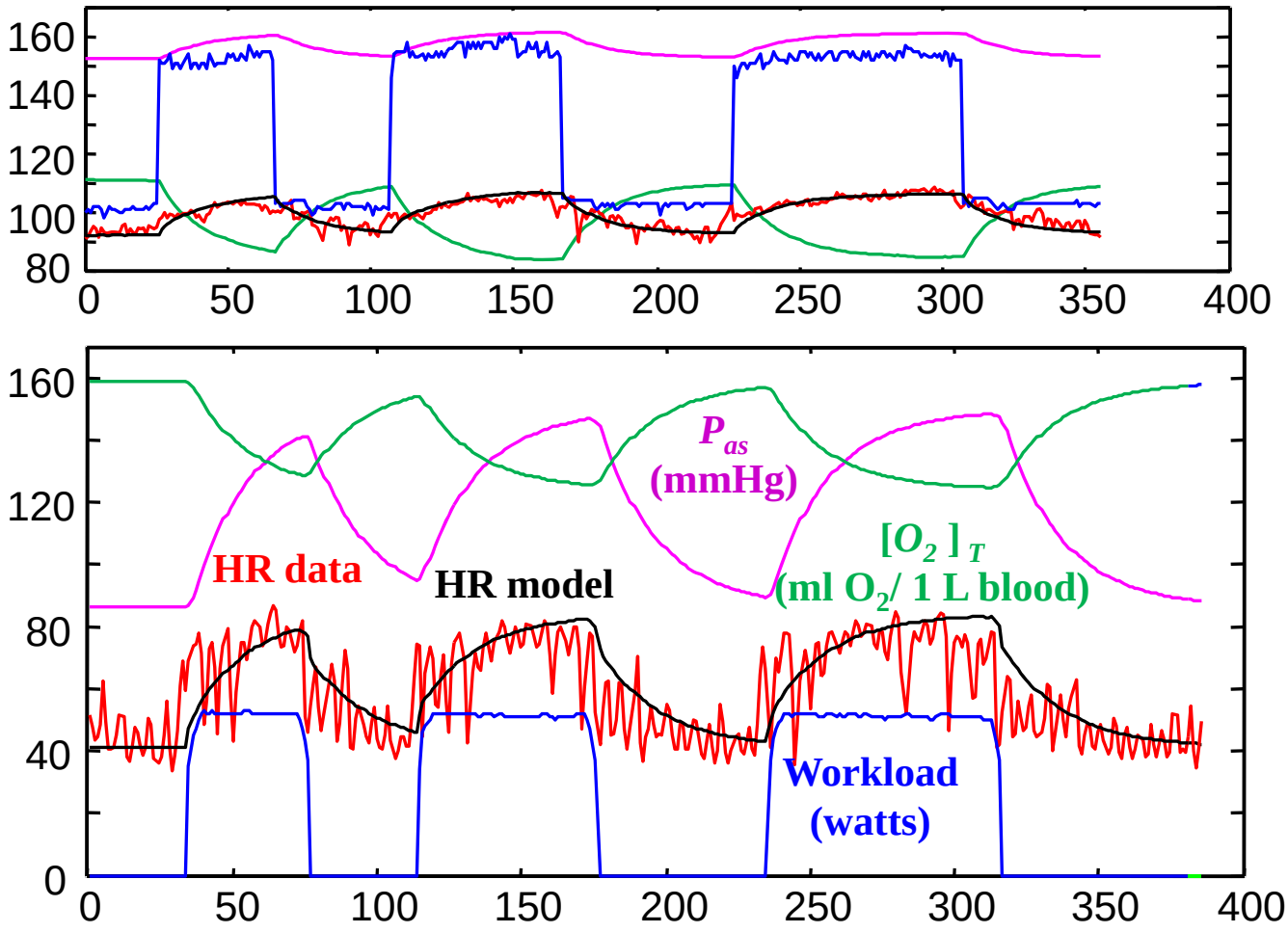

Figure S8: Subject #1's data: optimal control model of response to two different workload (blue) demands, approximately square waves of 0-50 watts (lower) and 100-150 watts (upper). For each data set, a first principle model with optimal controller is simulated with workload as input (blue) and HR (black) as output, which can be compared with HR data (red). Simulations of blood pressure (P_{as}, purple) and tissue oxygen saturation ($[O_2]_T$, green) are consistent with the literature but were not measured.

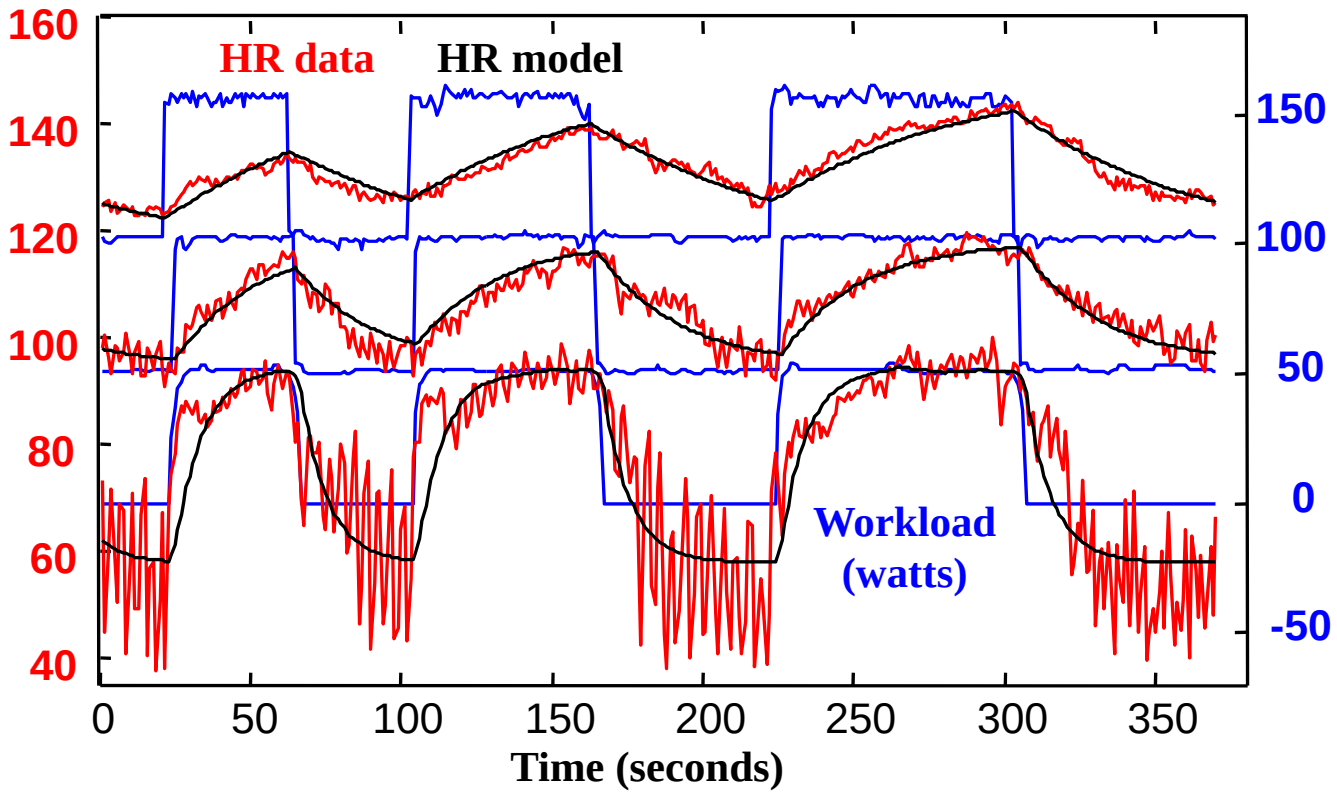

Figure S9: Subject #2 performed three separate experiments of less than 6 minutes each on a cycle ergometer. HR (left axis, red) is plotted for three different workload demands (right axis, blue). The workload profiles are similar but shifted square waves of 0-50 watts (lower), 50-100 watts (middle), and 100-150 watts (upper). A one state linear dynamic ("black box") model with 3 parameters (different for each case) was fit using workload input and HR output. The optimal parameter values (a, b, c)≈ (-0.11, 0.079, 6.54) at 0 watts differ greatly from those at 50 watts (-0.375, 0.017, 2.63) and at 100 watts (-0.014, 0.0095, 0.62). Simulations of these 3 different models with the 3 corresponding workload inputs are in black. Breathing was spontaneous (not controlled), and SpO_2 was essentially constant throughout.

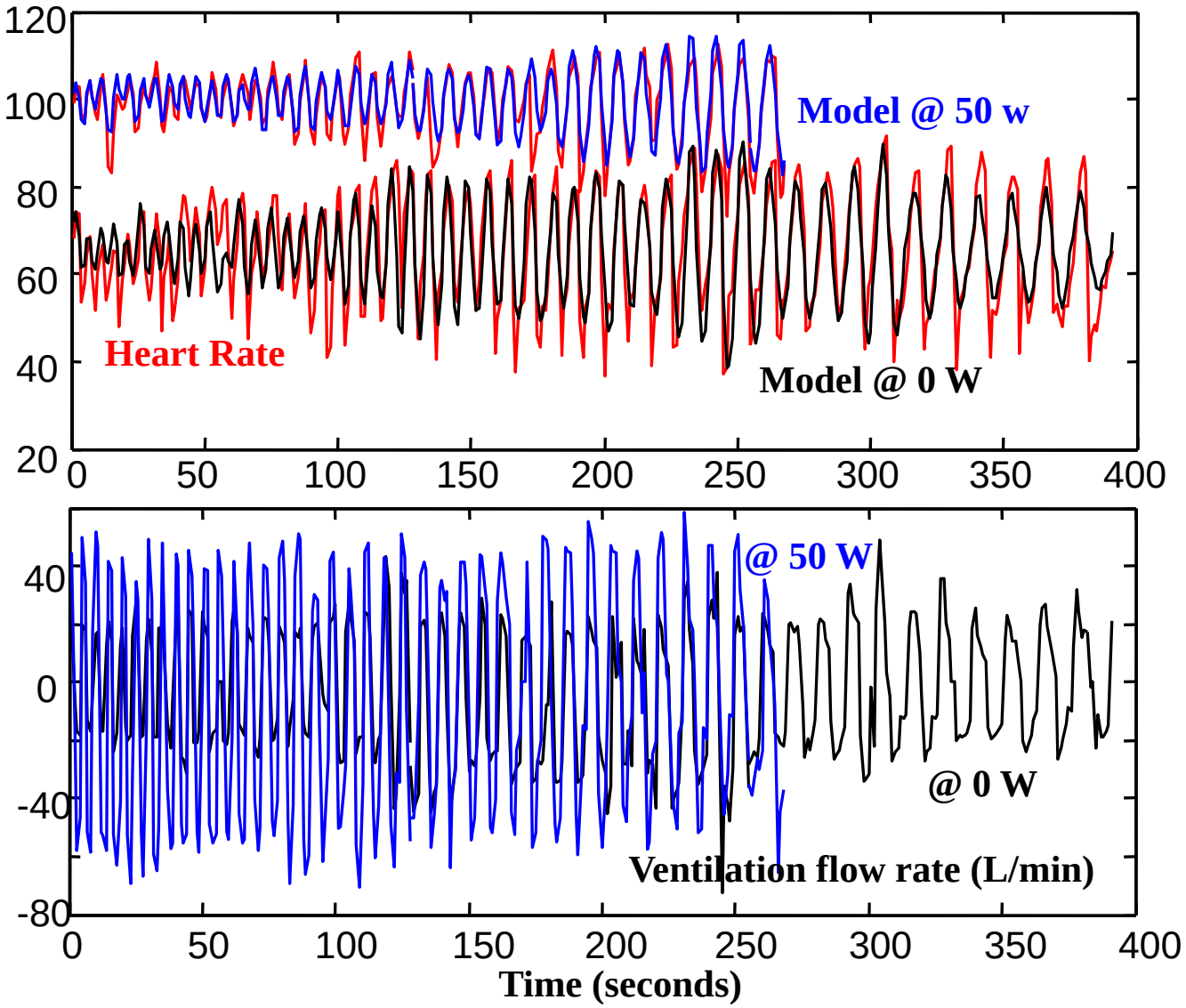

Figure S10: Subject #2's data: two experiments with input of controlled frequency sweeps in ventilation flow rate (lower plot) with fixed background workload demand of 0 watts (black) or 50 watts (blue). Subject #2 controlled breathing to follow a preprogrammed frequency sweep that spanned the natural breath frequencies at these workload levels. The ventilation data are raw speed of inhalation and exhalation at the mouthpiece. For each data set, a second order linear model was fit with airflow rate input (lower plot) and HR output (upper, data in red). Simulations of HR are in upper plot for 0 watts (black) and 50 watts (blue).

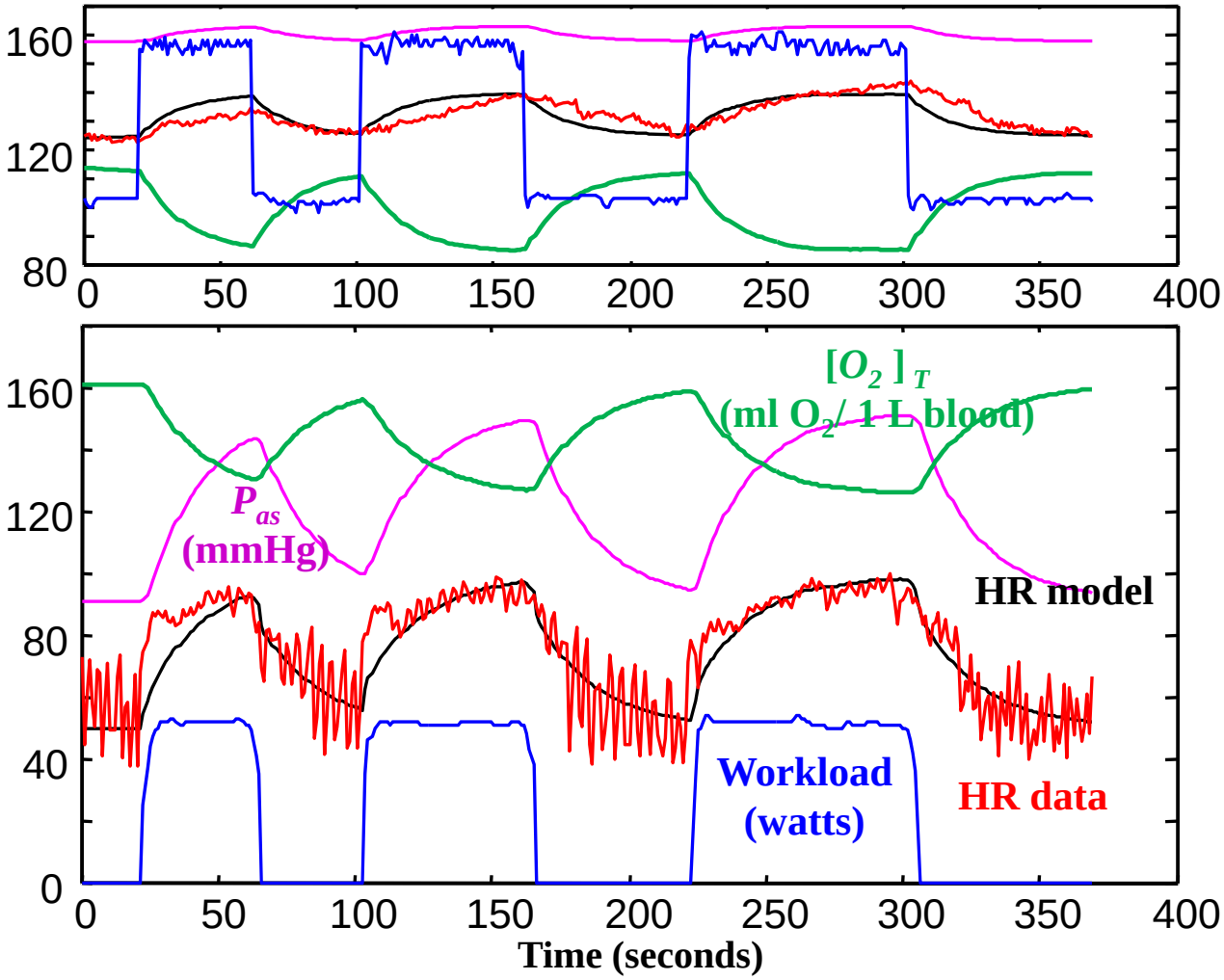

Figure S11: Subject #2's data: optimal control model of response to two different workload (blue) demands, approximately square waves of 0-50 watts(lower) and 100-150 watts (upper). For each data set, a first principle model with optimal controller is simulated with workload as input (blue) and HR (black) as output, which can be compared with HR data (red). Simulations of blood pressure (P_{as}, purple) and tissue oxygen saturation ($[O_2]_T$, green) are consistent with the literature but were not measured.

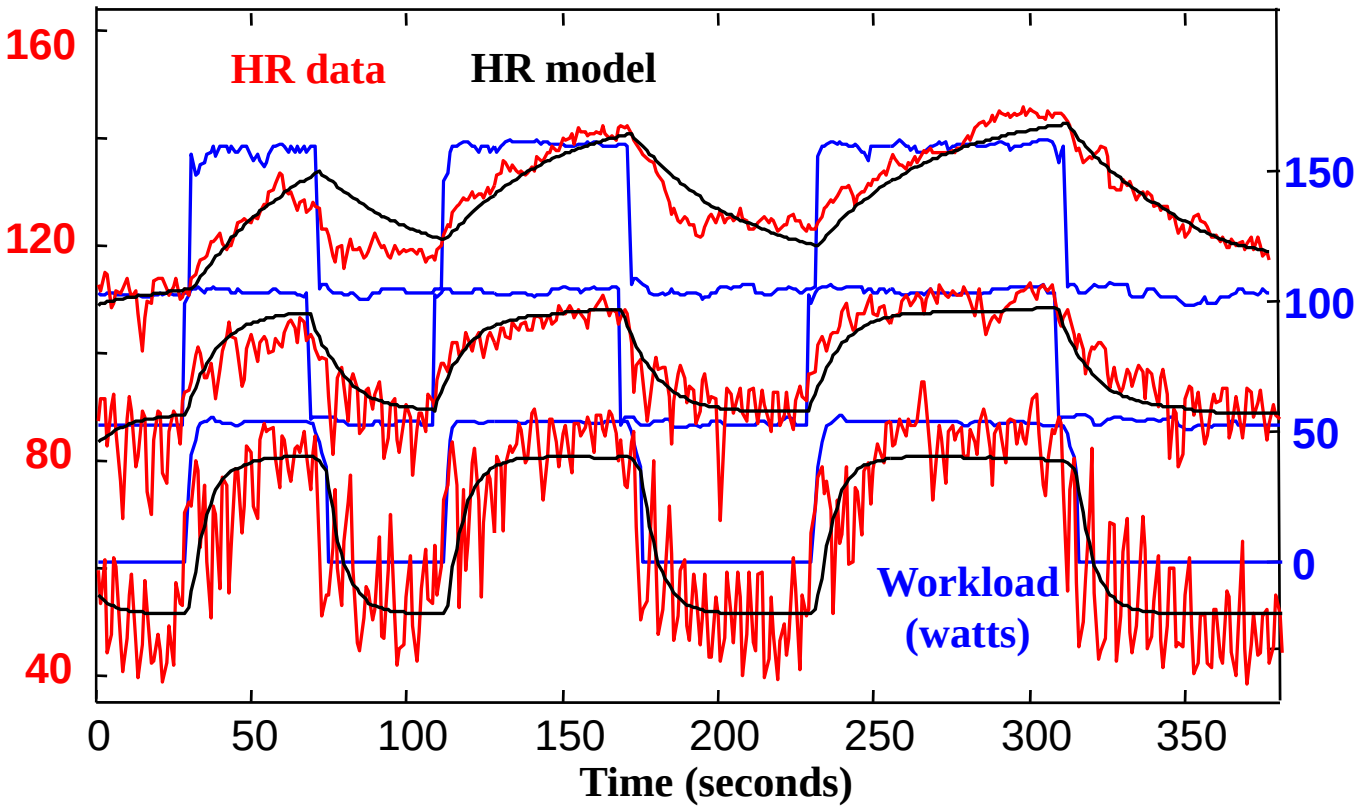

Figure S12: Subject #3 performed three separate experiments of less than 6 minutes each on a cycle ergometer. HR (left axis, red) is plotted for three different workload demands (right axis, blue). The workload profiles are similar but shifted square waves of 0-50 watts (lower), 50-100 watts (middle), and 100-150 watts (upper). A one state linear dynamic ("black box") model with 3 parameters (different for each case) was fit using workload input and HR output. The optimal parameter values (a, b, c)≈ (-0.18, 0.10, 9.47) at 0 watts differ greatly from those at 50 watts (-0.098, 0.037, 6.70) and at 100 watts (-0.028, 0.015, 1.59). Simulations of these 3 different models with the 3 corresponding workload inputs are in black. . Breathing was spontaneous (not controlled), and SpO_2 was essentially constant throughout.

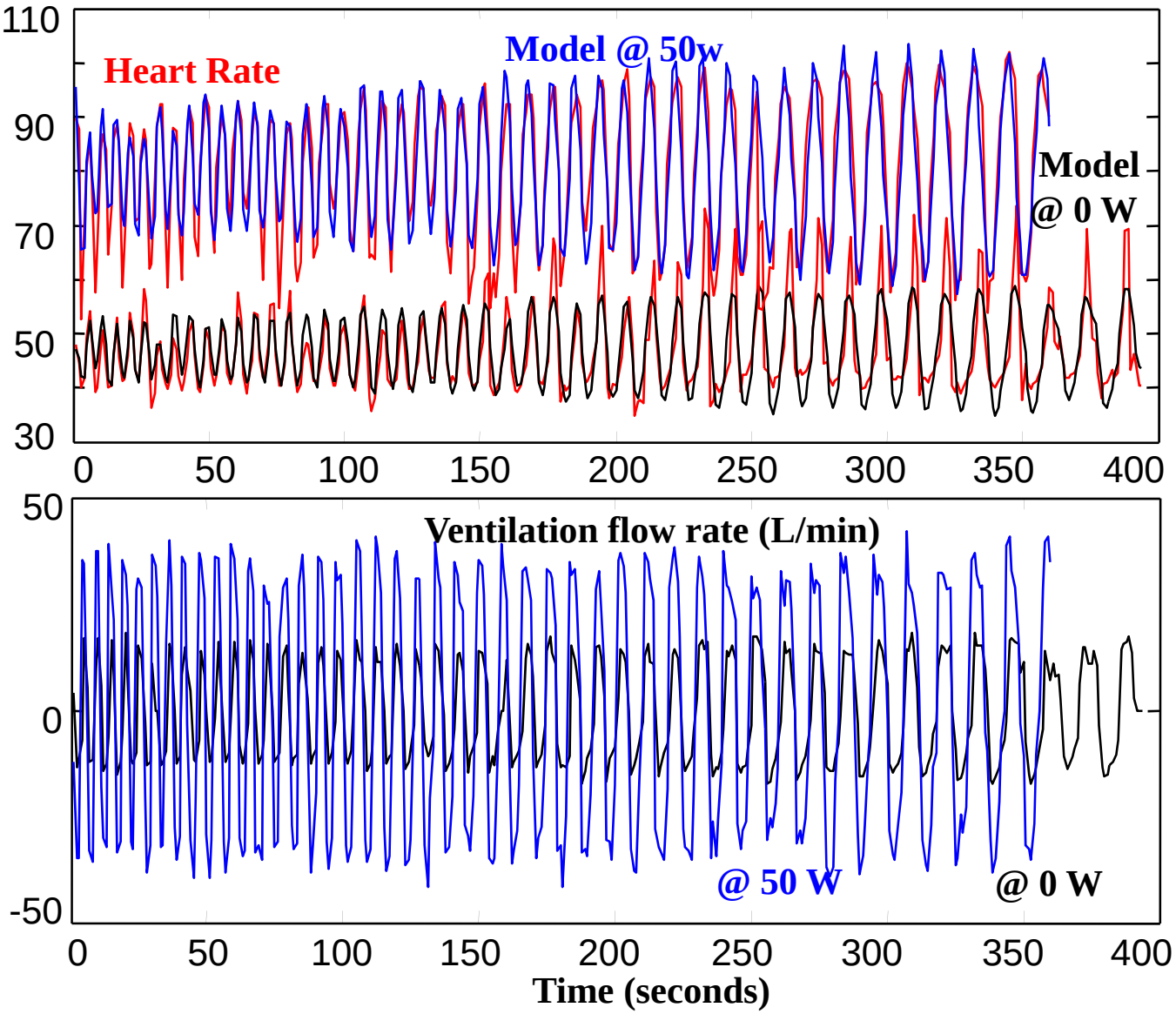

Figure S13: Subject #3's data: two experiments with input of controlled frequency sweeps in ventilation flow rate (lower plot) with fixed background workload demand of 0 watts (black) or 50 watts (blue). Subject #3 controlled breathing to follow a preprogrammed frequency sweep that spanned the natural breath frequencies at these workload levels. The ventilation data are raw speed of inhalation and exhalation at the mouthpiece. For each data set, a second order linear model was fit with airflow rate input (lower plot) and HR output (upper, data in red). Simulations of HR are in upper plot for 0 watts (black) and 50 watts (blue).

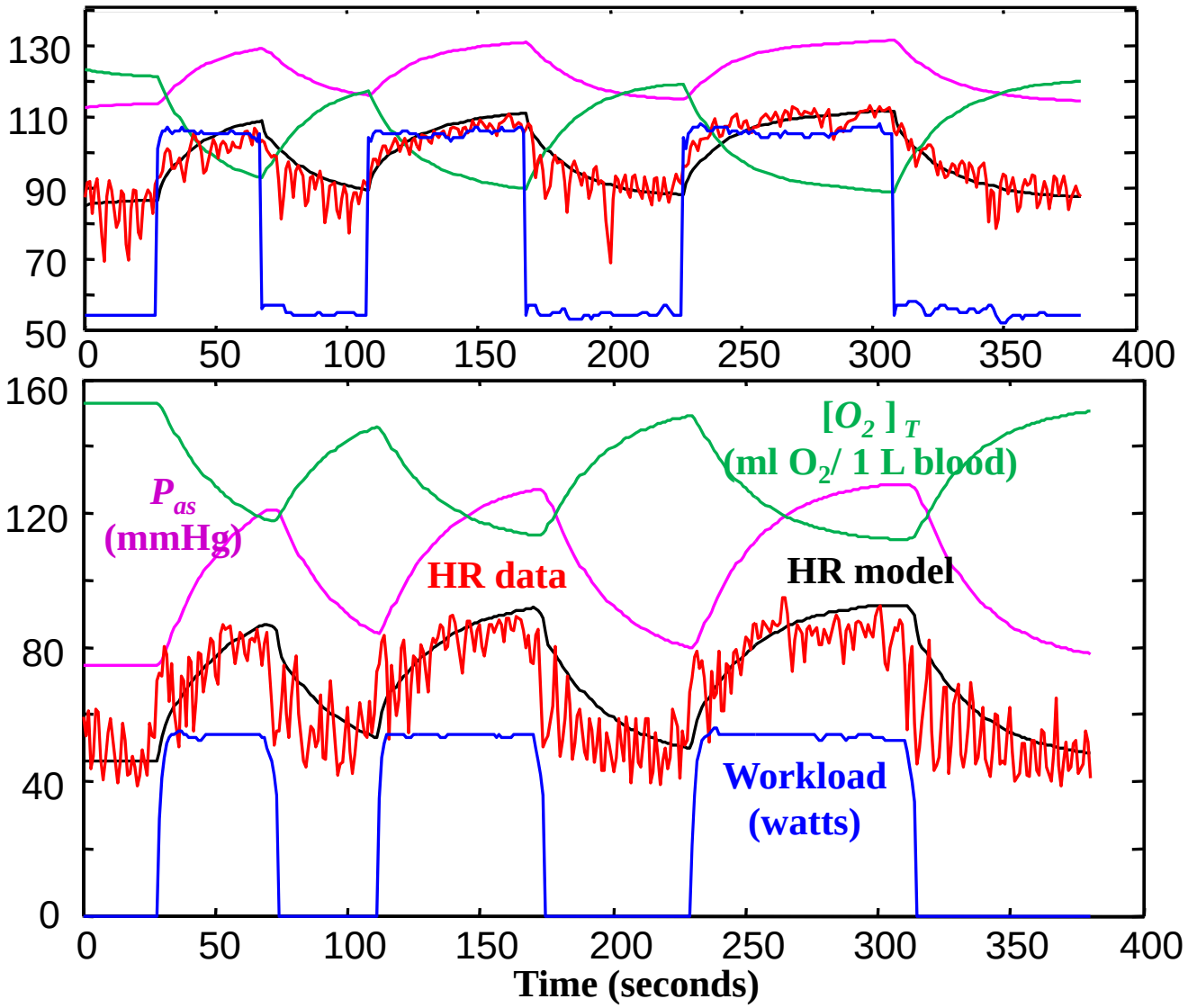

Figure S14: Subject #3's data: optimal control model of response to two different workload (blue) demands, approximately square waves of 0-50 watts (lower) and 50-100 watts (upper). For each data set, a first principle model with optimal controller is simulated with workload as input (blue) and HR (black) as output, which can be compared with HR data (red). Simulations of blood pressure (*BP*, purple) and tissue oxygen saturation ($[O_2]_T$, green) are consistent with the literature but were not measured.

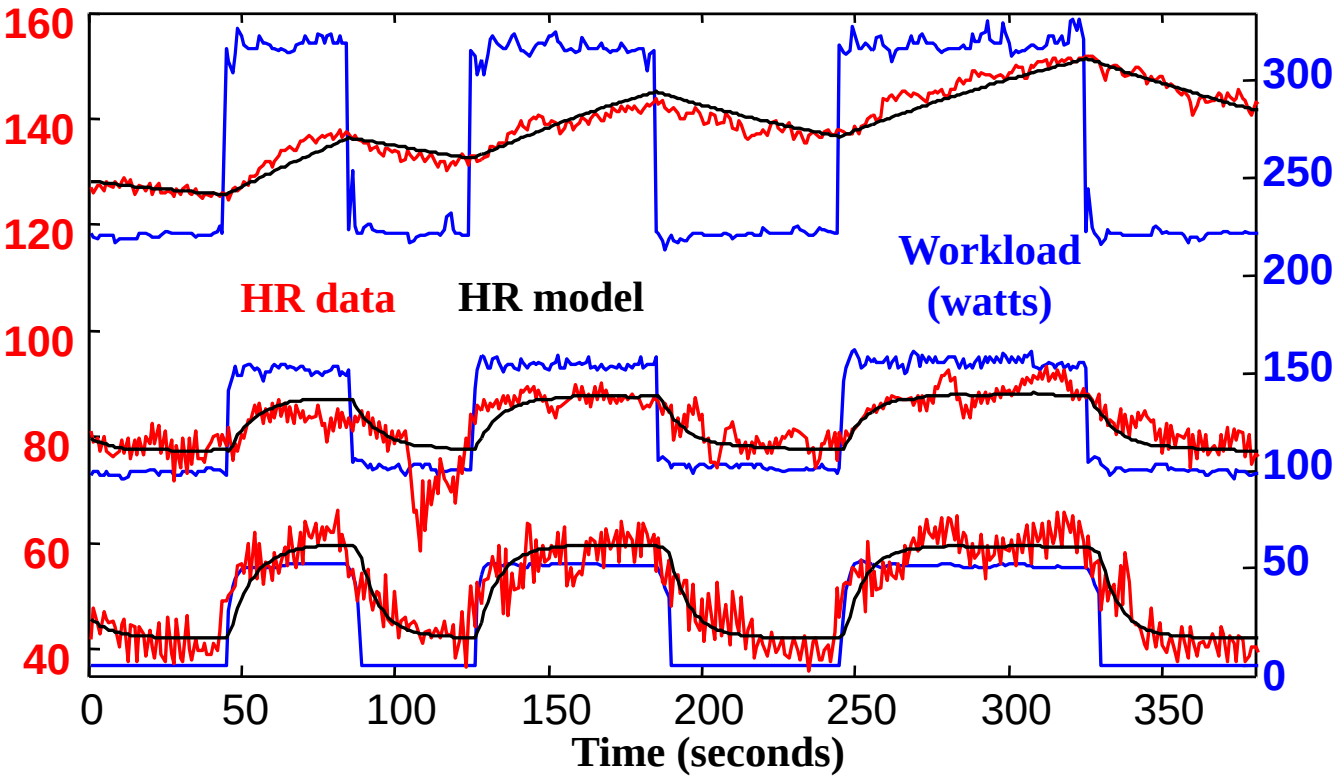

Figure S15: Subject #4 performed three separate experiments of less than 6 minutes each on a cycle ergometer. HR (left axis, red) is plotted for three different workload demands (right axis, blue). The watt profiles are similar but shifted square waves of 0-50 watts (lower), 100-150 watts (middle), and 220-320 watts (upper). A one state linear dynamic ("black box") model with 3 parameters (different for each case) was fit using watts input and HR output. The optimal parameter values (a, b, c)≈ (-0.15, 0.051, 6.41) at 0 watts differ greatly from those at 100 watts (-0.12, 0.023, 7.32) and at 220 watts (-0.0064, 0.0036, -0.039). Simulations of these 3 different models with the 3 corresponding workload inputs are in black. Breathing was spontaneous (not controlled), and SpO_2 was essentially constant throughout.

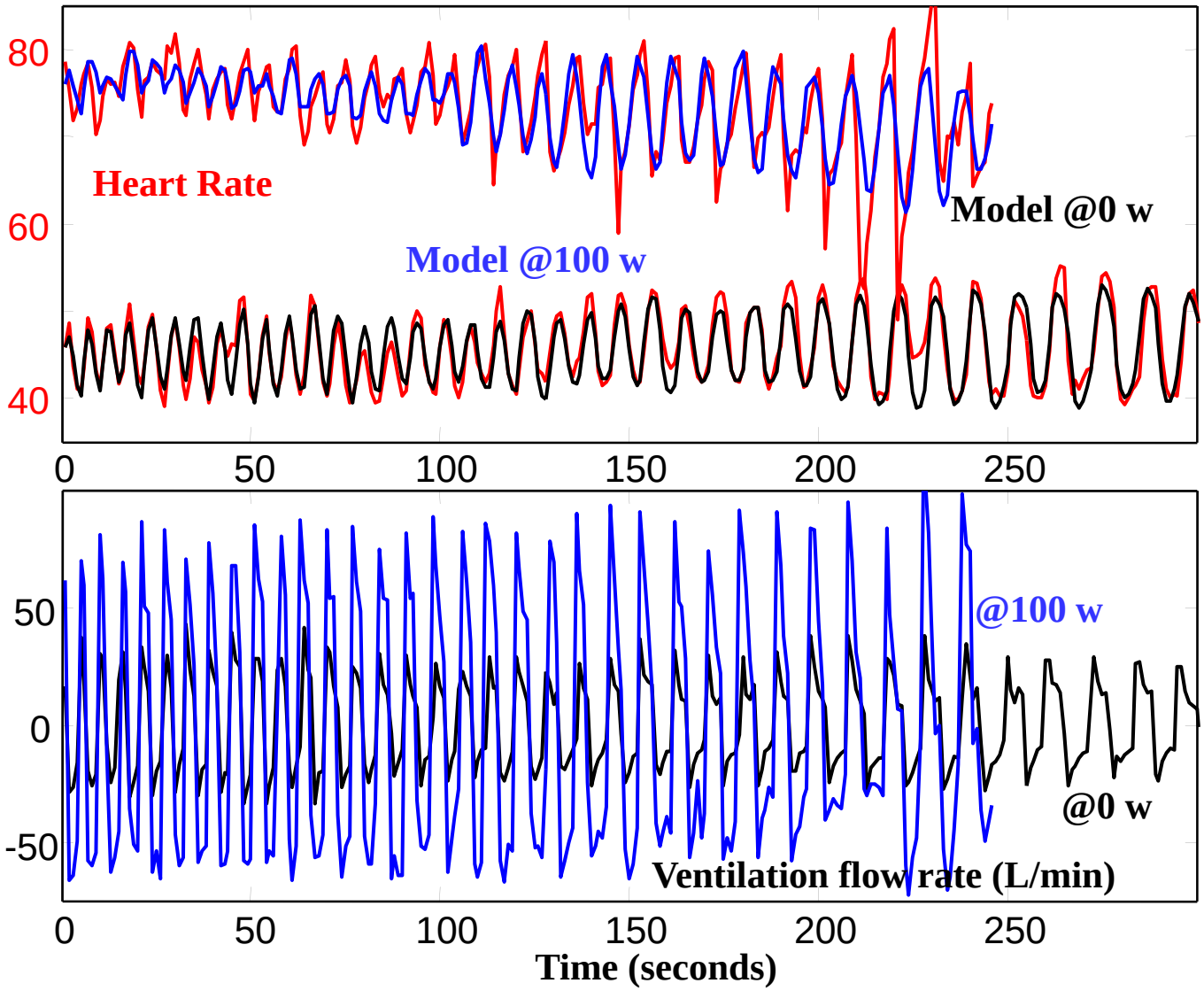

Figure S16: Subject #4's data: two experiments with input of controlled frequency sweeps in ventilation flow rate (lower plot) with fixed background workload demand of 0 watts (black) or 100 watts (blue). Subject #4 controlled breathing to follow a preprogrammed frequency sweep that spanned the natural breath frequencies at these workload levels. The ventilation data are raw speed of inhalation and exhalation at the mouthpiece. For each data set, a second order linear model was fit with airflow rate input (lower plot) and HR output (upper, data in red). Simulations of HR are in upper plot for 0 watts (black) and 100 watts (blue).

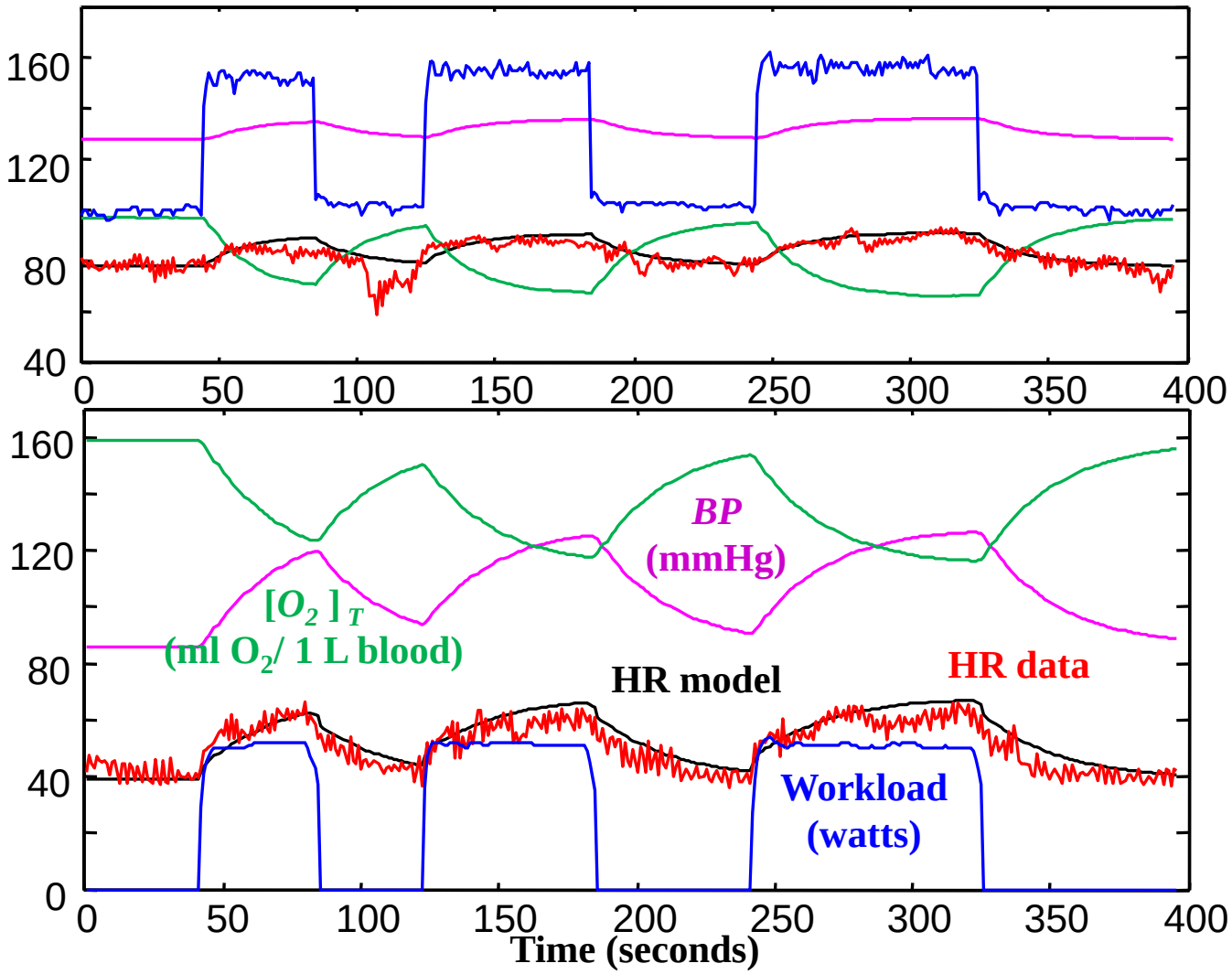

Figure S17: Subject #4's data: optimal control model of response to two different workload (blue) demands, approximately square waves of 0-50 watts (lower) and 100-150 watts (upper). For each data set, a first principle model with optimal controller is simulated with workload as input (blue) and HR (black) as output, which can be compared with HR data (red). Simulations of blood pressure (*BP*, purple) and tissue oxygen saturation ($[O_2]_T$, green) are consistent with the literature but were not measured.

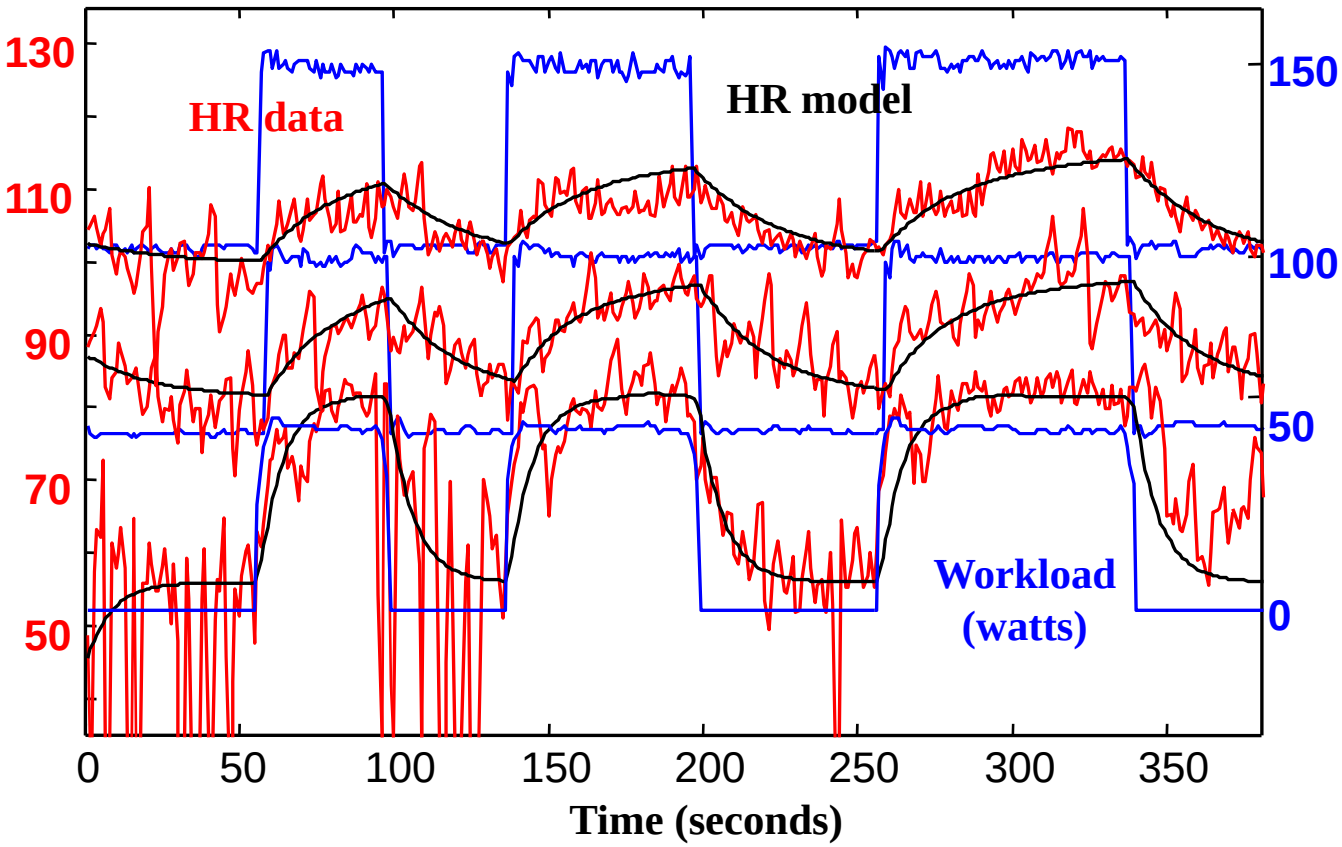

Figure S18: Subject #5 performed three separate experiments of less than 6 minutes each on a cycle ergometer. HR (left axis, red) is plotted for three different workload demands (right axis, blue). The workload profiles are similar but shifted square waves of 0-50 watts (lower), 50-100 watts (middle), and 100-150 watts (upper). A one state linear dynamic ("black box") model with 3 parameters (different for each case) was fit using workload input and HR output. The optimal parameter values (a, b, c)≈ (-0.13, 0.064, 7.05) at 0 watts differ greatly from those at 50 watts (-0.045, 0.015, 2.93) and at 100 watts (-0.036, 0.01, 2.54). Simulations of these 3 different models with the 3 corresponding workload inputs are in black. Breathing was spontaneous (not controlled), and SpO_2 was essentially constant throughout.

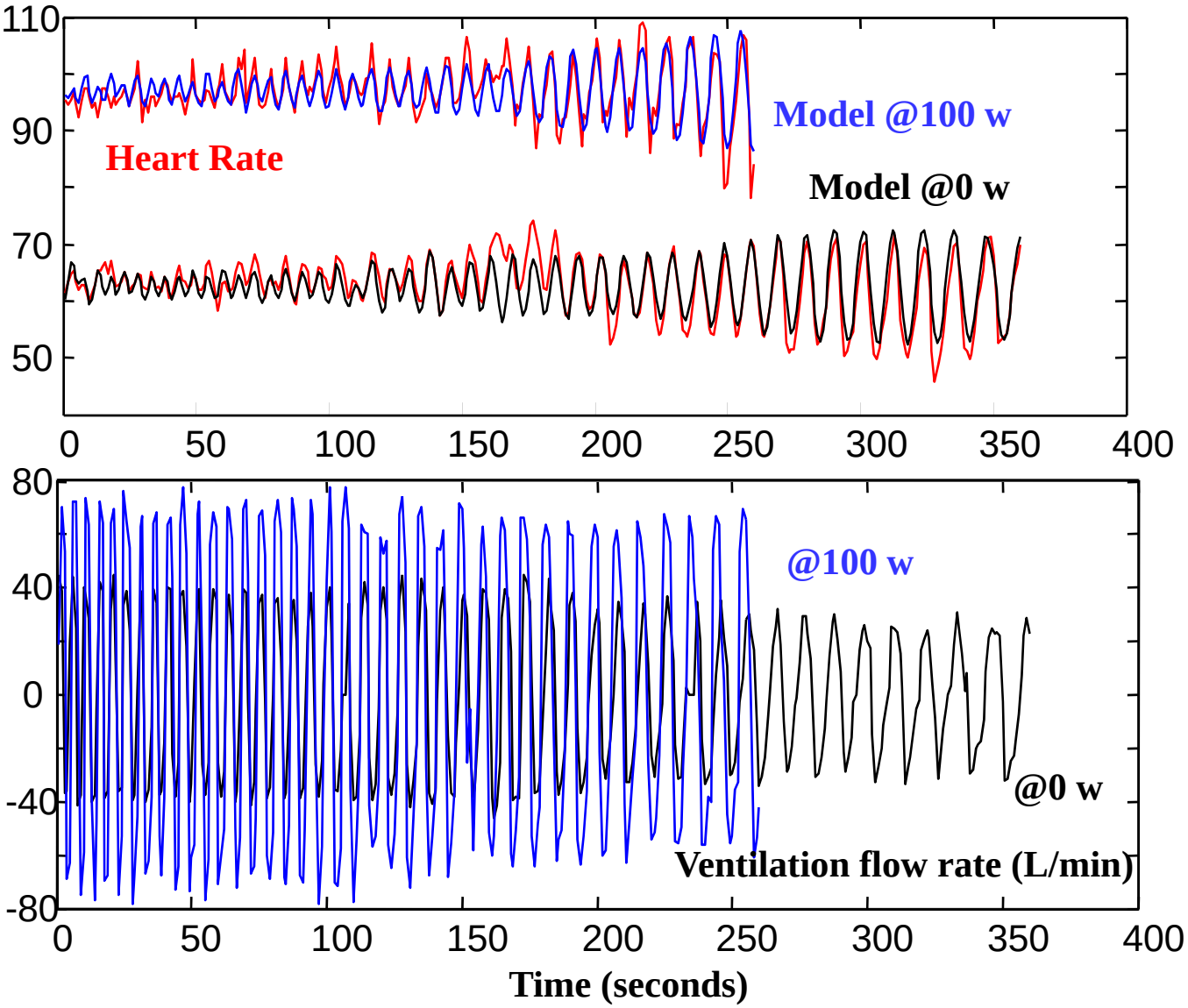

Figure S19: Subject #5's data: two experiments with input of controlled frequency sweeps in ventilation flow rate (lower plot) with fixed background workload demand of 0 watts (black) or 50 watts (blue). Subject #5 controlled breathing to follow a preprogrammed frequency sweep that spanned the natural breath frequencies at these workload levels. The ventilation data are raw speed of inhalation and exhalation at the mouthpiece. For each data set, a second order linear model was fit with airflow rate input (lower plot) and HR output (upper, data in red). Simulations of HR are in upper plot for 0 watts (black) and 50 watts (blue).

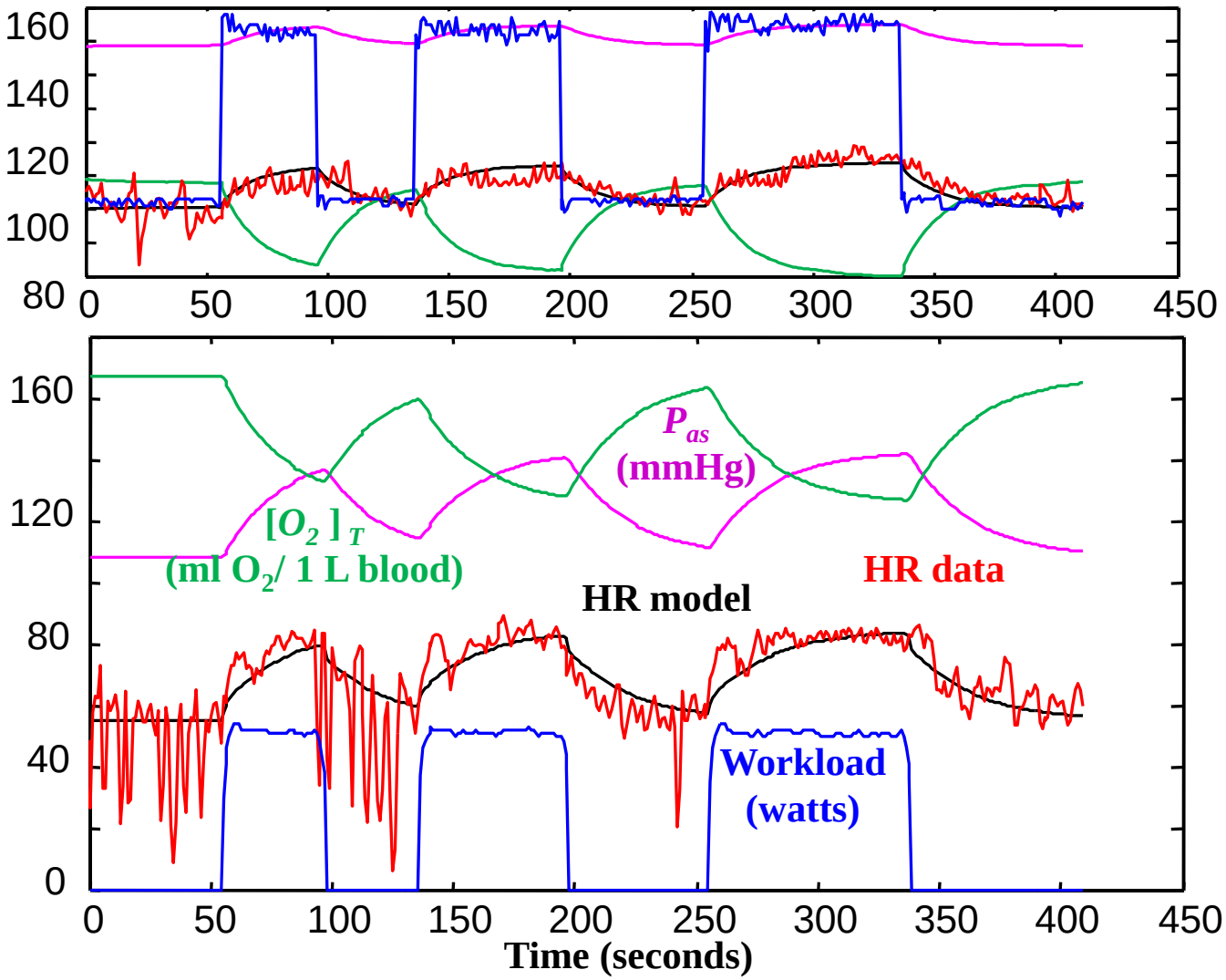

Figure S20: Subject #5's data: optimal control model of response to two different workload (blue) demands, approximately square waves of 0-50 watts (lower) and 100-150 watts (upper). For each data set, a first principle model with optimal controller is simulated with workload as input (blue) and HR (black) as output, which can be compared with HR data (red). Simulations of blood pressure (P_{as}, purple) and tissue oxygen content ($[O_2]_T$, green) are consistent with the literature but were not measured.

III. Nonlinear Dynamic Model from System ID

We have shown that overall HR response to a broad workload is a nonlinear system, by using experiments with limited watts range and individual but different linear models. To explore global nonlinear models, we did experiments including exercise levels between 0 watts and 150 watts and found a piecewise linear model to fit the data. The following two figures show two experiments data and the corresponding fitting results. In both of the fittings, we use piecewise 1st order linear model with 2 linear pieces and 7 parameters, which is shown as follows:

$$\begin{aligned} \Delta H(t) &= a_1 H(t) + b_1 W(t) + c_1; \quad \text{when } h(t) \le \bar{H} \\ \Delta H(t) &= a_2 H(t) + b_2 W(t) + c_2; \quad \text{otherwise} \end{aligned}$$

Constants $(a_1, b_1, c_1, a_2, b_2, c_2, \bar{H})$ are fitted to minimize the mean squared error between $H(t)$ and HR data. In SI-Section IV: *Cross Validation*, we show how validation results change with number of pieces and we claim that 2 linear pieces are an optimal balance between model order, fit, and cross validation. Wider watts ranges would require more states and nonlinearities.

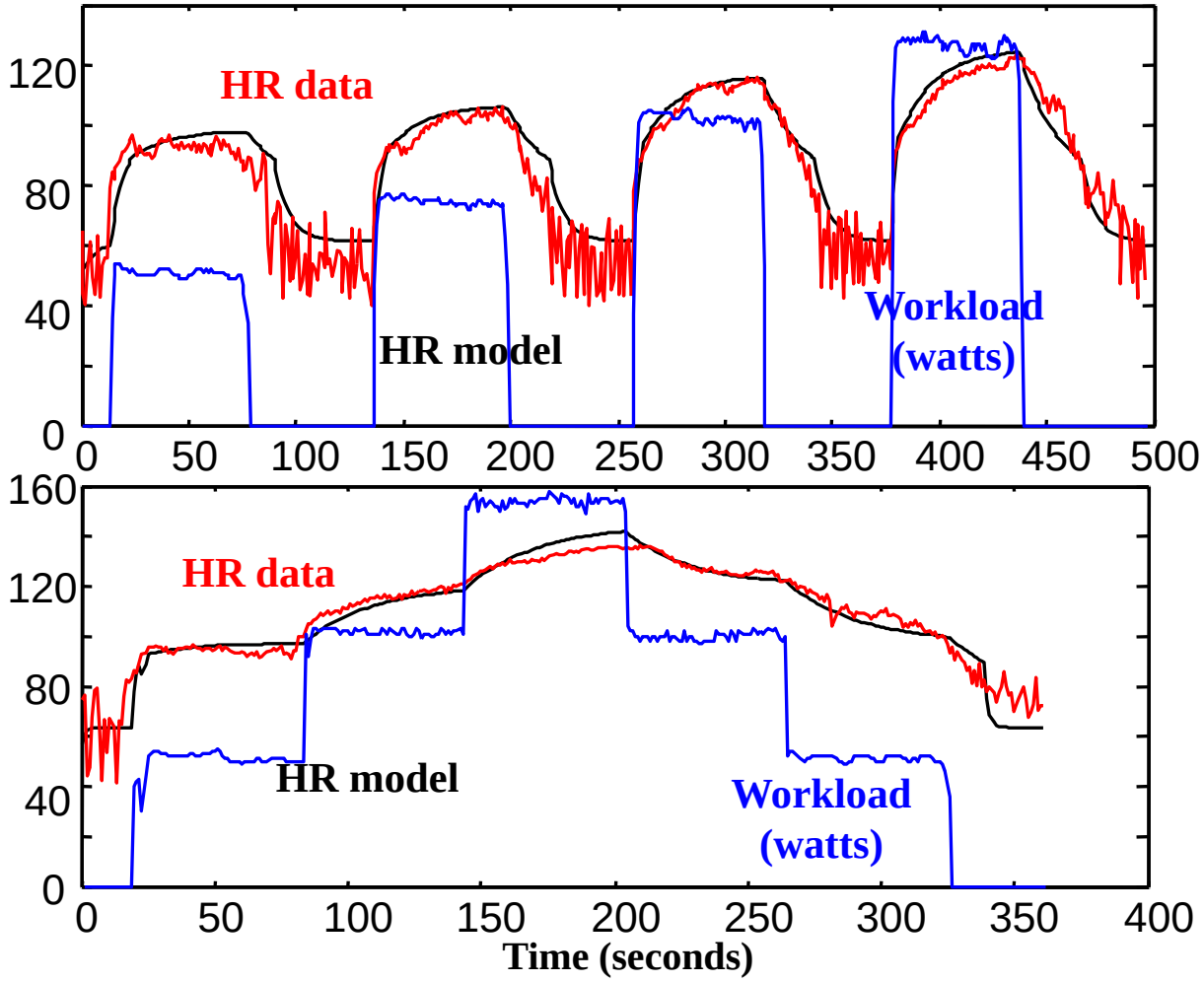

Figure S21: Subject #2 performed two separate experiments of less than 6 minutes each on a cycle ergometer. HR (left axis, red) is plotted for 2 different watts demands (blue) including exercise levels between 0 watts and 150 watts. For each experiments, a piecewise 1st order linear model ("black box") with 2 linear pieces and 7 parameters was fit using workload input and HR output. Simulations of this model with the 2 watts input are in black.

IV. Cross Validation

In this section, we perform cross validation on our models: the linear system identification model, the first principle model, and the nonlinear system identification model. In each cross validation, a subject performs two different exercise tests with different but comparable workload demands. We fit our models by using one set of experimental data (i.e. training data) and use the fitted models to perform prediction on the other set of experimental data (i.e. validation data). Moreover, in cross validation for linear system identification models and nonlinear system identification models, we fit and simulate different models with different complexities and we show how validation results correlate with the model complexities.

1. Linear System Identification Model

Fig. S22 shows an example of validation result for linear system identification models on two data sets. The subject performed two separate experiments of less than 8 minutes each on a cycle ergometer including exercise levels between 50 watts and 100 watts. We use the upper data set (called as data set 1) as training data and the lower data set (called as data set 2) as validation data. In Fig. S22, a 1st order linear dynamic ("black box") model (i.e., $\Delta h = ah + bW + c$) with 3 parameters (a,b,c) was fit using data set 1 with workload input and HR output and simulations of this model is done with the 2 workload inputs. From the simulation results, we can see that the 1st order linear dynamic model can predict HR response to workloads well.

To further address the over-fitting issue and to study how validation results correlate with model complexities, we then fit and simulate different models with different complexities on the two data sets. Fig. S23 and Table S1 shows the cross validation results. The classes of models we compare in the figure are: linear static model, 1st order linear dynamic model, 2nd order linear dynamic model, 3rd order linear dynamic model, and 4th order linear dynamic model. For each class of models, we do three different fittings: using data set 1 to fit a model; using data set 2 to fit a model; using both data set 1 and data 2 fit a model. Then we use those models to simulate both of the two data sets and calculate the corresponding root mean squared errors on those data sets. The root mean squared error is defined as:

$$\mathrm{RMS} = \sqrt{\frac{1}{N}\sum_{t=1}^{N}\left(H(t) - HR(t)\right)^2}$$

where $H(t)$ and $HR(t)$ are respectively the simulated and the measured heart rate at time point t, and N

is the total number of time points. The three markers in each line in Fig. S23 for each class of models show the simulated errors using the corresponding three different fitted models, which are, from left to right, the fitted model using data set 1, the fitted model using the two data sets; the fitted model using data set 2. Not surprisingly, Fig. S23 and Table S1 show that the RMS error becomes roughly smaller with increased fit complexity on the training data. However, the marginal benefit starts diminishing as the model complexity increases; moreover, the validation RMS error starts to increase if the model is very complex (see the RMS error for 3rd linear dynamic model and RMS error for 4th linear dynamic model).

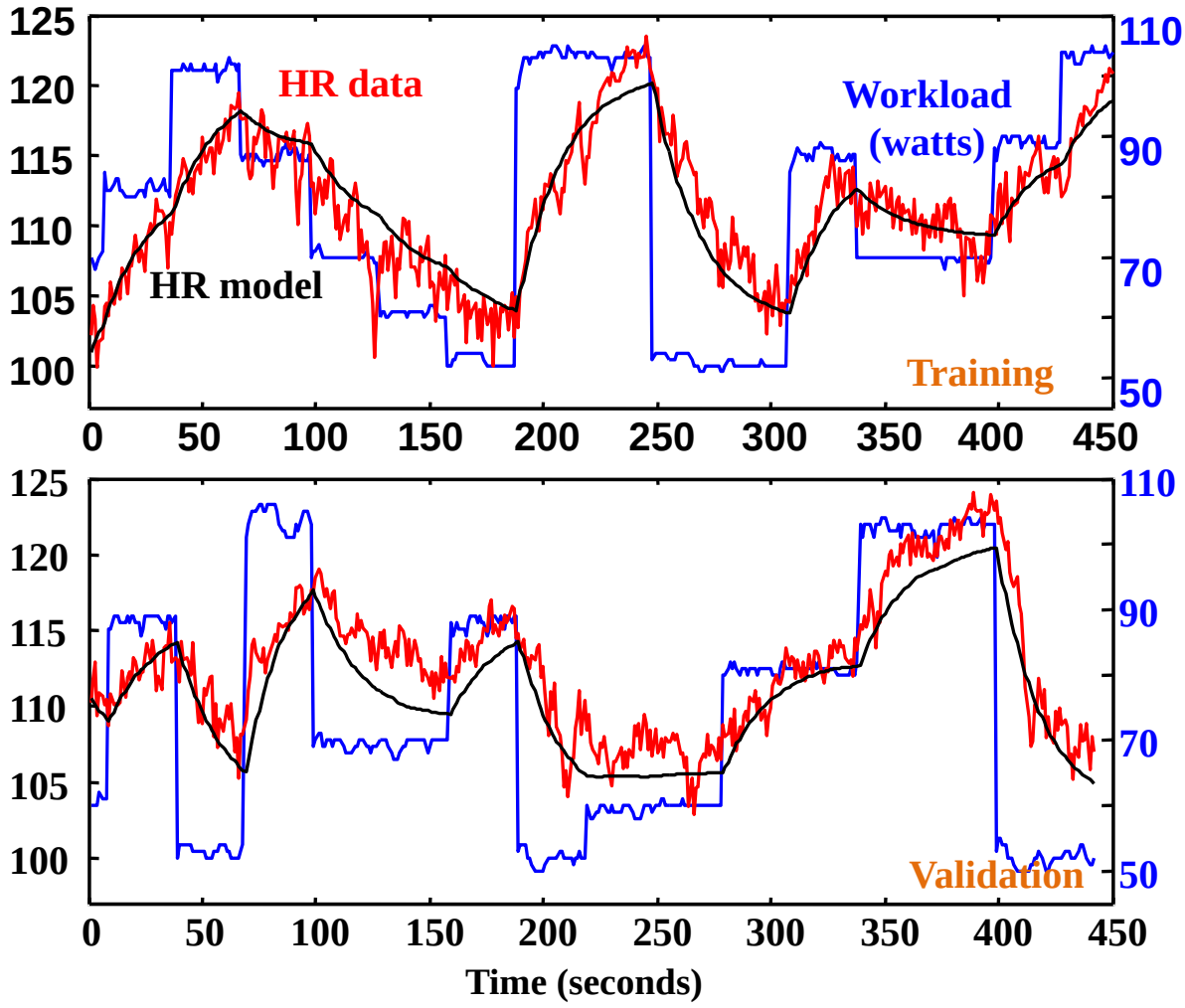

Figure S22: Subject #2 performed two separate experiments of less than 8 minutes each on a cycle ergometer including exercise levels between 50 watts and 100 watts. HR (left axis, red) is plotted for two different workload demands (right axis, blue). A 1st order linear dynamic ("black box") model (i.e., $\Delta H = aH + bW + c$) with 3 parameters (a,b,c) was fit using the upper exercise data with workload input and HR output. Simulations of this model with the 2 workload inputs are in black.

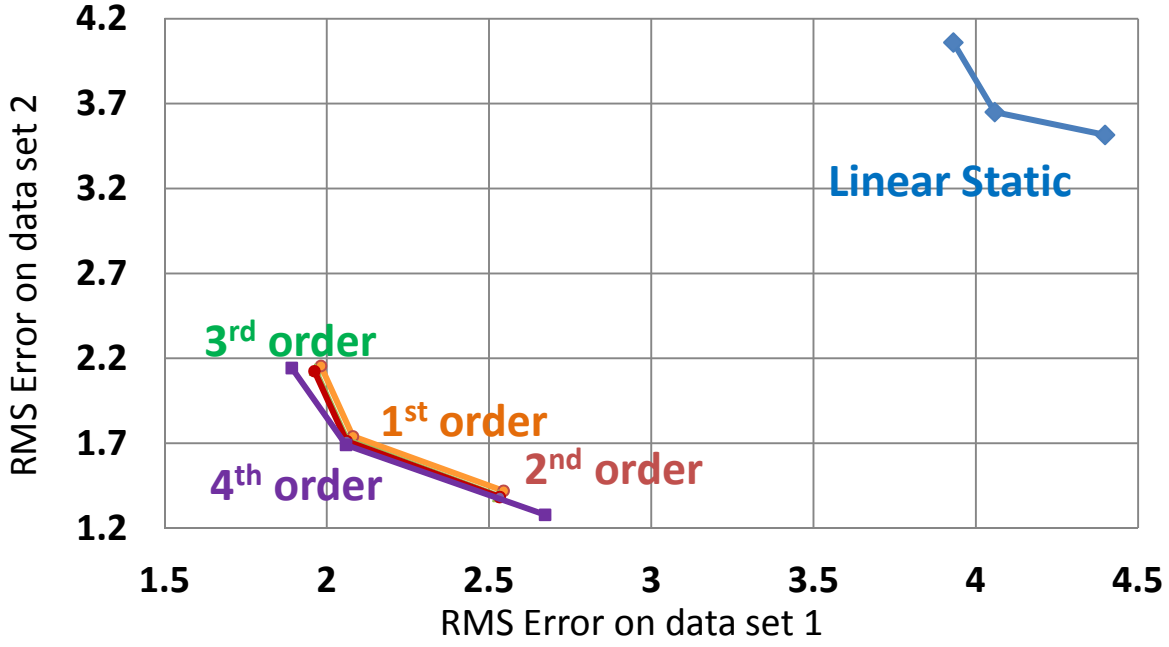

Figure S23: In this figure, we use the two experiments' data in Supplementary Figure 18 to show how validation results correlate with the complexity of the model. We call the upper experiment data set in Fig. S22 data set 1 and the lower one data set 2. The classes of models we compare in the figure are: linear static model (blue), 1st order piecewise linear models with 1 piece (orange), 2 pieces (red), 3 pieces (green), and 4 pieces (purple). For each class of models, we do three different fittings: using data set 1 to fit a model; using data set 2 to fit a model; using both data set 1 and data 2 fit a model. Then we use those models to simulate the two data sets and calculate the corresponding mean squared errors on those data sets. The mean squared error is defined as:

$$\text{error}=\sqrt{\frac{1}{N}\sum_{t=1}^{N}\left(H(t)-HR(t)\right)^2}$$

where *H(t)* and *HR(t)* are respectively the simulated and the measured heart at time point *t*, and *N* is the total number of time points. The three markers in each line for each class of models show the simulated errors using the corresponding three different fitted models, which are, from left to right, the fitted model using data set 1, the fitted model using the two data sets; the fitted model using data set 2. From this plot, we claim that 2 linear pieces are an optimal balance between model order, fit, and cross validation.

Table S1, RMS error of cross validation for linear dynamic models

	Training	Validation	Validation	Training	Fitting together	
	Data 1	Data2	Data 1	Data2	Data 1	Data2
Linear Static	3.9306	4.0603	4.3980	3.5160	4.0582	3.6503
1st order linear dynamic	1.9818	2.1553	2.5446	1.4197	2.0803	1.7402
2nd order linear dynamic	1.8200	1.4347	2.5289	1.3900	2.0631	1.7190
3rd order linear dynamic	1.8034	1.4297	2.4782	1.3815	1.8654	1.4323
4th order linear dynamic	1.8006	1.4285	2.5198	1.3487	1.7689	1.4194

2. First Principle Model

Figure S24 shows the validation result for the 1st principle model. We still use data set 1 as training data and data set 2 as validation data. The three tradeoff parameters (q_p, q_O, q_H) in the cost function of the first principle model are fitted using data set 1 (training data) with workload input and HR output. This first principle model is simulated for each data set with workload as input (blue) and HR (black) as output, which can be compared with measured HR data (red). Simulations of blood pressure (P_{as}, purple) and tissue oxygen saturation ($[O_2]_T$, green) are consistent with the literature but were not measured. . From the simulation results, we can see that the 1st principle model can predict HR response to workloads well.

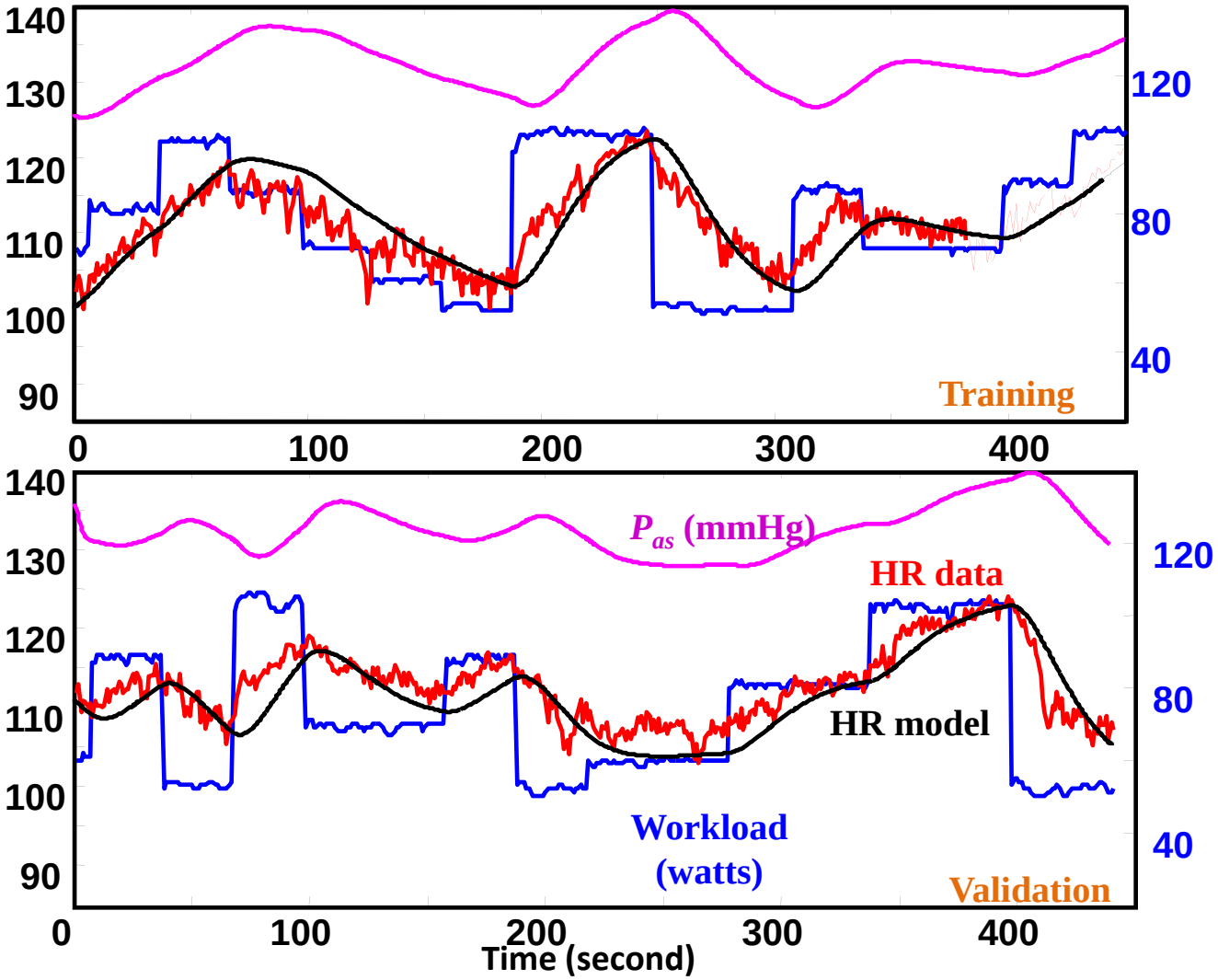

Figure S24: Subject #2's data using first principle models: optimal control model of response to the two different workload (blue) demands including exercise levels between 50 watts and 100 watts. The three tradeoff parameters in the cost function of the first principle model are fitted using the upper exercise data (i.e. training data) with workload input and HR output. This first principle model is simulated for each data set with workload as input (blue) and HR (black) as output, which can be compared with measured HR data (red). Simulations of blood pressure (P_{as}, purple) are consistent with the literature but were not measured.

3. Nonlinear System Identification Model—Piecewise Linear Dynamic Model

We carried out cross validation on the nonlinear system identification model by repeating the same process as that for the linear system identification model in SOM-Section IV-1. We call the upper data set in Figure S21 data set A and the lower data set data set B. A piecewise 1st order linear model ("black box") with 2 linear pieces and 7 parameters was fit using data set 1 with workload input and HR output and simulations of this model is done with the 2 workload as inputs. Then we fit and simulate different models with different complexities on the two data sets to study how validation results correlate with model complexities which is shown in Fig. S25-26.

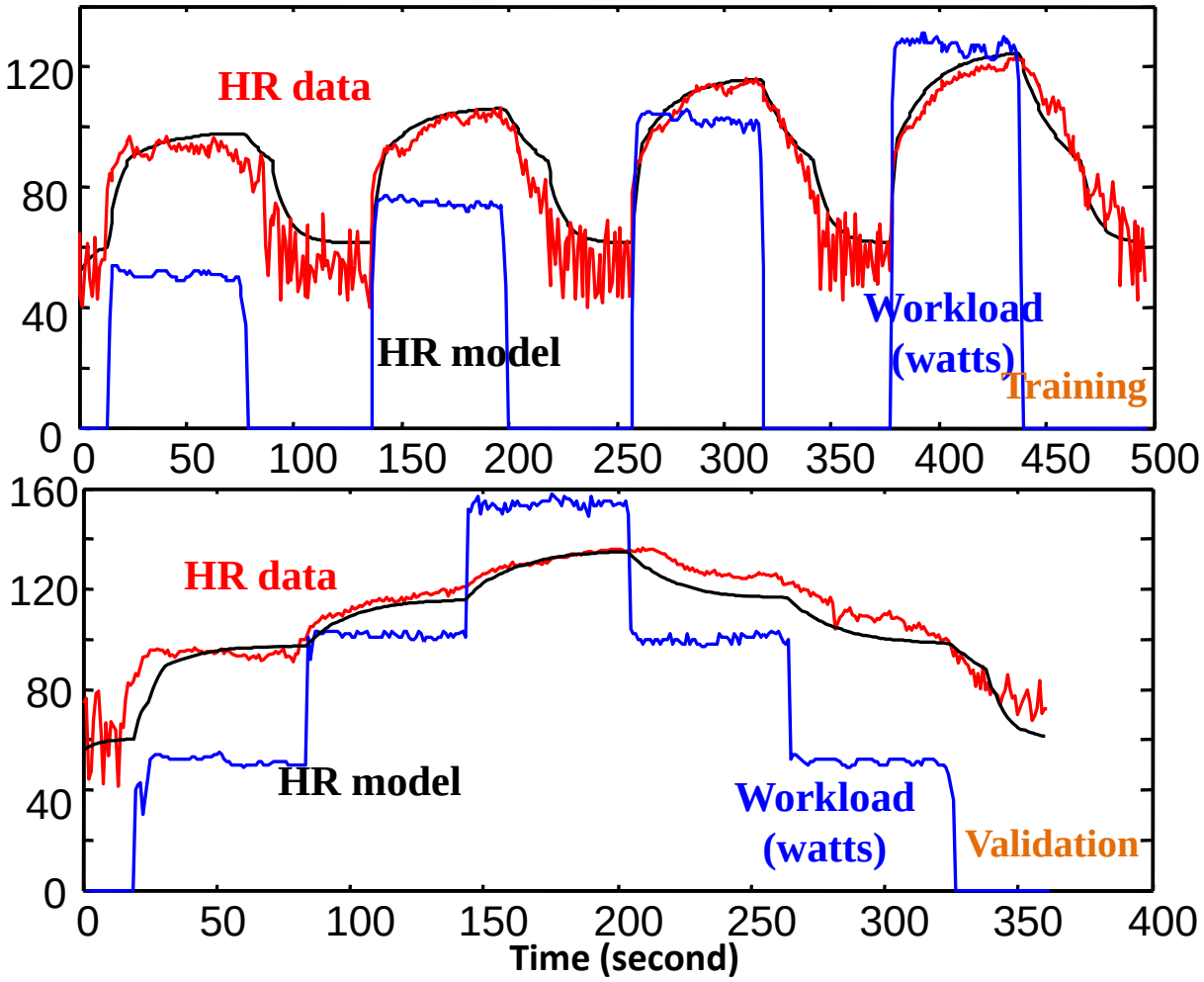

Figure S25: Validation results for the nonlinear system identification model. HR (left axis, red) is plotted for two different workload demands (right axis, blue). We use the upper data set (called as data set A) in Fig. S21 as training data and the lower data set (called as data set B) as validation data. A piecewise 1st order linear model ("black box") with 2 linear pieces and 7 parameters was fit using the training data with workload input and HR output. Simulations of this model with the 2 workload inputs are in black.

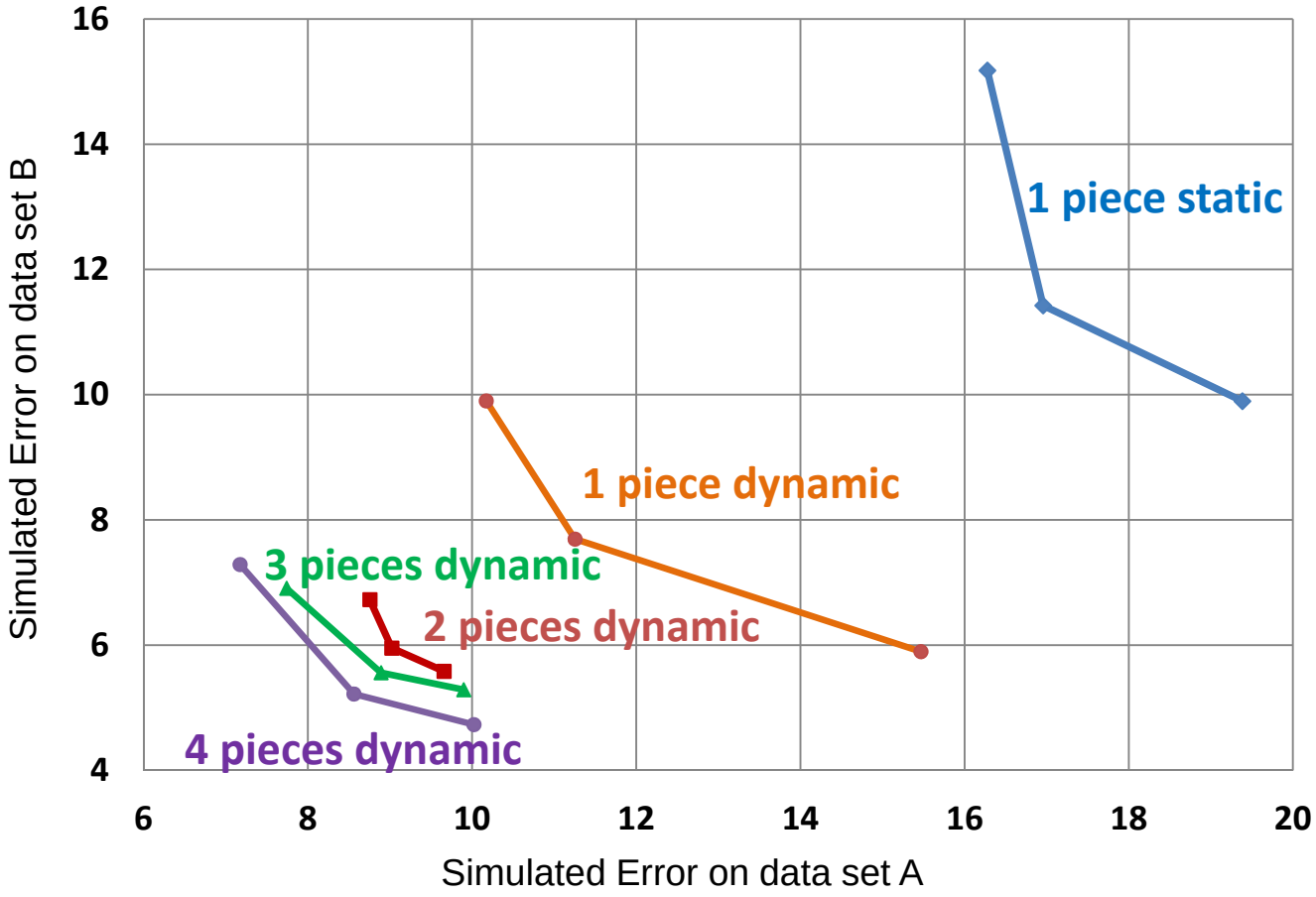

Figure S26: In this figure, we use the two experiments' data in Fig. S21 to show how validation results correlate with the complexity of the model. We call the upper experiment data set in Fig.S21 as data set A and the lower one as data set B. The classes of models we compare in the figure are: 1 piece linear static model (blue), 1st order piecewise linear models with 1 piece (orange), 2 pieces (red), 3 pieces (green), and 4 pieces (purple). For each class of models, we do three different fittings: using data set 1 to fit a model; using data set 2 to fit a model; using both data set 1 and data 2 fit a model. Then we use those models to simulate the two data sets and calculate the corresponding mean squared errors on those data sets. The mean squared error is defined as:

$$\text{error}=\sqrt{\frac{1}{N}\sum_{t=1}^{N}\left(H(t)-HR(t)\right)^2}$$

where *H(t)* and *HR(t)* are respectively the simulated and the measured heart at time point *t*, and *N* is the total number of time points. The three markers in each line for each class of models show the simulated errors using the corresponding three different fitted models, which are, from left to right, the fitted model using data set 1, the fitted model using the two data sets; the fitted model using data set 2. From this plot, we claim that 2 linear pieces are an optimal balance between model order, fit, and cross validation.

V. Tables S2-S4:

Table S2: Parameters value

Parameter	Value	Parameter	Value	Parameter	Value
c_{as}	0.01016(L/mmHg)	R_p	0.5(mmHg min/L)	V_{T,O_2}	6.0 (L)
c_{vs}	0.6500(L/mmHg)	R_{s0}	6.5(mmHg min/L)	$[O_2]_a$	0.2 (L O_2/L blood)
c_{ap}	0.0361(L/mmHg)	A	18(mmHg min /L)	ρ	0.012(L/min/watt)
c_{vp}	0.1408(L/mmHg)	V_{tot}	5.0580 (L)	M_0	0.36 (L/min)

Table S3: Parameters value for cardio output

Subject	Parameter	Value	Parameter	Value
1	c_l	0.03(L/mmHg)	c_r	0.05(L/mmHg)
2	c_l	0.025(L/mmHg)	c_r	0.045(L/mmHg)
3	c_l	0.02(L/mmHg)	c_r	0.04(L/mmHg)
4	c_l	0.032 (L/mmHg)	c_r	0.052(L/mmHg)
5	c_l	0.03 (L/mmHg)	c_r	0.05(L/mmHg)

Table S4: q value for dynamic 1st principle model

Subject		Parameter	Value	Parameter	Value	Parameter	Value
1	0-50 watts	q_{as}	30	q_{O_2}	100000	q_H	1
	100-150watts	q_{as}	65	q_{O_2}	100000	q_H	15
2	0-50 watts	q_{as}	30	q_{O_2}	100000	q_H	1
	100-150watts	q_{as}	80	q_{O_2}	100000	q_H	35
3	0-50 watts	q_{as}	40	q_{O_2}	100000	q_H	5
	50-100watts	q_{as}	65	q_{O_2}	100000	q_H	15
4	0-50 watts	q_{as}	45	q_{O_2}	100000	q_H	1
	100-150watts	q_{as}	85	q_{O_2}	100000	q_H	50
5	0-50 watts	q_{as}	40	q_{O_2}	100000	q_H	1
	100-150watts	q_{as}	80	q_{O_2}	100000	q_H	40

VI: System Identification Techniques

1 Parametric Dynamical Model

A discrete linear time invariant (LTI) system with single input single output (SISO) is applied to approximate causal dependencies between various physiological variables in our study. This LTI system is parameterized in the following obervable canonical form:

$$\begin{aligned} \Delta x[k] \triangleq x[k+1] - x[k] &= Ax[k] + Bu[k] + [0, \ldots, 0, 1]^T c \\ y[k] &= [1, 0, \ldots, 0]x[k] \qquad\qquad k = 0, 1, 2, ... \end{aligned} \tag{SI-16}$$

where A is parameterized as

$$A = \begin{bmatrix} a_1 & 1 & 0 & 0 & \cdots & 0 \\ a_2 & 0 & 1 & 0 & \cdots & 0 \\ \vdots & \vdots & \vdots & \vdots & \ddots & \vdots \\ a_n & 0 & 0 & 0 & \cdots & 0 \end{bmatrix}.$$

$x[k] \in \mathbb{R}^n$,$u[k] \in \mathbb{R}$ and $y[k] \in \mathbb{R}$ denote the state, input and output of the system, respectively. The unknowns of the system are $A \in \mathbb{R}^{n \times n}$, $B \in \mathbb{R}^n$, $c \in \mathbb{R}$ and $x[0] \in \mathbb{R}^n$, the initial condition. Given a positive discrete time instant N and two sequences of scalar data from measured physiological variables, $\hat{\boldsymbol{u}} := \{\hat{u}[k]\}_{k=0}^{N-1}$ and $\hat{\boldsymbol{y}} := \{\hat{y}[k]\}_{k=0}^{N-1}$, we estimate the unknowns of the system $(A, B, c, x[0])$ so that when $\hat{\boldsymbol{u}}$ is applied as input to the system, the resulting output, $\boldsymbol{y}$, is close to $\hat{\boldsymbol{y}}$.

The advantage of using observable canonical form is that it reduces unknown parameter dimension and thus reduces computational complexity without loss of generality. Moreover, we have observed that this form is empirically more accurate at fitting stiff systems than other state-space techniques.

2 Parameter Estimation

Denote $E_c = [0, \ldots, 0, 1]^T$ and $E_r = [1, 0, \ldots, 0]$. Using the parameterization given above, the solution to (SI-16) for a given input signal $\hat{\boldsymbol{u}}$ is

$$y[k] = E_r A^{k-1} x[0] + \sum_{i=1}^{k-1} E_r A^{k-1-i} B u(i) + \sum_{i=1}^{k-1} E_r A^{k-1-i} E_c c$$

for $k = 0, 1, 2, \ldots, N-1$. The parameter estimation problem can then be stated as follows. For fixed n, we wish to find A, B, c and $x[0]$ that minimize the mean squared error between $\boldsymbol{y}$ and $\hat{\boldsymbol{y}}$, i.e. we wish to minimize

$$V\left(A, B, c, x[0]\right) = \frac{1}{N} \sum_{k=0}^{N-1} \frac{1}{2} \left[\hat{y}[k] - y[k]\right]^2.$$

Letting $\varphi_A[k] = \begin{bmatrix} E_r A^{k-1} & \sum_{i=1}^{k-1} u(i) E_r A^{k-1-i} & \sum_{i=1}^{k-1} E_r A^{k-1-i} E_c \end{bmatrix}$ and $\xi = \begin{bmatrix} x[0]^T & B^T & c \end{bmatrix}^T$, the solution to (SI-16) can be rewritten as $y[k] = \varphi_A^T[k]\xi$, and the quadratic cost criterion becomes

$$V\left(A, \xi\right) = \frac{1}{N} \sum_{k=0}^{N-1} \frac{1}{2} \left[\hat{y}[k] - \varphi_A^T[k]\xi\right]^2.$$

From this it is clear that if $\varphi_A[k]$ is known for $k = 0, \ldots, N-1$, minimizing V with respect to ξ is a linear least-squares problem that has a unique global minimum and can be solved efficiently. Since $\boldsymbol{\varphi_A}$ only depends on A, for fixed A, $\varphi_A[k]$ can be computed for $k = 0, \ldots, N-1$. Thus, our approach to the parameter estimation problem is to employ a direct search over the space parameterizing A, wherein the cost associated with a point A_0 is $\min_{\xi} V(A_0, \xi)$. Since A is parameterized in observable canonical form, the direct search occurs over an n-dimensional space. Letting $\hat{Y} = \begin{bmatrix} \hat{y}[0] & \hat{y}[1] & \cdots & \hat{y}[N-1] \end{bmatrix}^T$ and $\Phi_A = \begin{bmatrix} \varphi_A[0] & \varphi_A[1] & \cdots & \varphi_A[N-1] \end{bmatrix}^T$ we have that, for fixed A,

$$\left(\Phi_A^T \Phi_A\right)^{-1} \Phi_A^T \hat{Y} = \arg\min_{\xi} V(A, \xi). \tag{SI-17}$$

Thus, the cost criterion used in the direct search for A can be written as

$$\overline{V}(A) = \frac{1}{N} \sum_{k=0}^{N-1} \frac{1}{2} \left[\hat{y}[k] - \varphi_A^T[k] \left(\Phi_A^T \Phi_A\right)^{-1} \Phi_A^T \hat{Y}\right]^2.$$

We use the Nelder-Mead simplex algorithm as our direct search method for estimating A. This is a nonlinear unconstrained optimization algorithm that attempts to minimize scalar-valued nonlinear functions using only function values, i.e. without gradient information. Because the objective $V(A)$ is nonconvex, we cannot guarantee that our estimate for A is globally optimal. Nonetheless, A is parametrized by relatively few variables, and our direct search is thus restricted to a low-dimensional space. We therefore expect that our method of eliminating parameters $(B, c, x[0])$ and then searching only for A provides a more optimal estimate than would be obtained via a joint optimization over $(A, B, c, x[0])$. Though the Nelder-Mead algorithm is not guaranteed to find the globally optimal A, we observe in practice that this direct search is insensitive to our initial search point. We suspect this is because we focus on 1st and 2nd oder LTI models, and the search space for A is consequently very low dimensional.